UR

OF

OCU

A

IE

UN

HIS

MEN

E

LA-UR -82-1396

Los Alamos National Laboratory is operated by the University of California for the United States Department of Energy under contract W-7405-ENG-36

TITLE THE THERMONUCLEAR MODEL FOR X-RAY TRANSIENTS

AUTHOR(S) R. K. Wallace , Los Alamos Scientific Laboratory
S. E. Woosley, Lick Observatory, Univ. of Calif. Santa Cruz
and
Lawrence Livermore National Laboratory, CA
Thomas A. Weaver Lawrence Livermore National Laboratory, CA

SUBMITTED TO ASTROPHYSICAL JOURNAL PROCEEDINGS of workshop "Accreting Neutron Stars", July 19-23, 1982.
Max-Planck Institute, Germany

Los Alamos Los Alamos National Laboratory
Los Alamos, New Mexico 87545

FORM NO 836 R4
ST NO 2629 5/81

THE THERMONUCLEAR MODEL FOR X-RAY TRANSIENTS[1]

R. K. WALLACE AND S. E. WOOSLEY

Lick Observatory, Board of Studies in Astronomy and Astrophysics

University of California, Santa Cruz

and

Lawrence Livermore National Laboratory

University of California

and

THOMAS A. WEAVER

Lawrence Livermore National Laboratory

University of California

Received _____

[1]Lick Observatory Bulletin, No. 911.

ABSTRACT

The thermonuclear evolution of a 1.41 $M_\odot$ neutron star accreting both solar and metal-deficient mixtures of hydrogen, helium, and heavy elements at rates ranging from about 10^{-11} to 10^{-10} $M_\odot$ per year is examined using a one-dimensional numerical model. The metal deficient compositions may result either from placement of the neutron star in a binary system with a Population II red giant or from gravitational settling of heavy ions in the accreted material. For such accretion rates and metallicities, hydrogen burning, mediated by the β-limited CNO cycle, is stable and leads to the accumulation of a thick helium layer with mass 10^{23} to 10^{25} g and temperature $0.7 \leq T_8 \leq 1.2$. Helium ignition occurs under extremely degenerate circumstances and is catastrophically violent. In the lower mass helium shells this runaway is propagated as a convective deflagration; for the thicker layers a detonation front is set up which steepens into a strong relativistic shock wave in the neutron star envelope. In all models greatly super-Eddington luminosities in the outer layers of the neutron star lead to a sustained epoch of radiatively driven mass loss. Observationally, such models may correspond to rapid x-ray transients. The hopeless prospect for constructing a one-dimensional model for γ-ray bursts without magnetic field confinement is discussed and uncertainties pointed out in the strong screening correction for the helium burning reaction.

Subject headings: stars: accretion - stars: neutron - X-rays: bursts

I. INTRODUCTION

Following the observation by Hansen and Van Horn (1975; see also Van Horn and Hansen 1974) that hydrogen and helium burning might occur in an unstable manner on the surface of an accreting neutron star, Woosley and Taam (1976) advanced a model for γ-ray and x-ray bursts based upon thermonuclear instability in carbon and helium shells respectively. A similar model for x-ray bursts based on hydrogen shell flashes was proposed independently by Maraschi and Cavaliere (1977). Since that time, extensive numerical calculations (Joss 1977, 1978, 1979, 1980, 1981; Joss and Li 1980; Taam 1980abc; Taam and Pinklum 1978, 1979; Lamb and Lamb 1978; Fugimoto, Hanawa, and Miyaji 1980) have shown the thermonuclear model to be particularly useful for interpreting the observed properties of Type I x-ray bursts (Lewin and Clark 1980).

Thus far, these numerical investigations, principally of helium flashes on neutron stars, have concentrated on scenarios that involve relatively high accretion rates (with the exception of Taam and Picklum 1978 and Van Horn and Hansen 1974), resulting in the accumulation of small helium layers ($\sim 10^{22}$ g; cf. Joss 1978). Since these calculations indicate a peak luminosity that is already near the Eddington value, it is reasonable to expect that the greater energy available from a more massive helium layer might yield an event having a longer timescale (Joss 1981). Rapid x-ray transients have been observed with duration from 10 s to a few hours (Cooke 1976; Schrijver et al. 1978), and one of the main purposes of this paper is to investigate the possibility of producing such long duration events within the context of the thermonuclear model.

Section II describes the results of our one-dimensional numerical calculations of neutron stars accreting material containing 0.004% to 2% heavy metals at rates of 10^{-11} to a few times 10^{-10} $M_\odot$/yr. Section III discusses some simple analytical methods that can be used to describe the basic physical principles involved. Section IV summarizes the major conclusions of the study, and the Appendix describes an improved formalism for determining the enhancement of nuclear reaction rates by electron screening.

II. RESULTS OF NUMERICAL CALCULATIONS

a) Physics of the Calculation

The present study of thermonuclear flashes was carried out using the KEPLER computer code developed by Weaver, Zimmerman, and Woosley (1978; henceforth WZW) to study advanced stages of stellar evolution. This one-dimensional Lagrangian code incorporates fully implicit hydrodynamics and radiation transport. It is essential that implicitly differenced hydrodynamics be employed for the proper tracking of dynamic events in the surface layers of a neutron star, since a substantial and interesting fraction of the star remains in hydrostatic equilibrium feeding energy either by acoustic waves (which may steepen into shocks), or by convective and radiative transport to another part of the star that is in rapid motion. Courant time-scale limitations would pose a severe difficulty in any attempt to use explicit hydrodynamics to study the problems we shall discuss here. An artificial viscosity was employed to mediate shock wave interactions, but the dynamic viscosity coefficient included only the quadratic term (i.e. $\eta_{ii} = 0$, $\ell_1 = 0$, and $\ell_2 = 1$ in equation [3] of WZW).

Nuclear energy generation was calculated using a 19 isotope nuclear reaction network (also implicitly differenced; see WZW). Full coupling including all relevant strong and electromagnetic reactions was incorporated for abundant nuclei from hydrogen to ^{56}Ni. Electron capture on ^{56}Ni was included and beta-limitation of the CNO cycle of hydrogen burn

ing was properly considered. Nuclear reaction rates were taken from Fowler, Caughlan, and Zimmerman (1975) and Woosley et al. (1978). Screening corrections were taken from Graboske et al. (1973; see also the Appendix), and neutrino loss rates from Beaudet, Petrosian and Salpeter (1967). An extensive reaction network of this type is essential for the present study where the temperature substantially exceeds 3×10^9 K.

A detailed model of time dependent convection based on mixing length theory was also employed, as was an equation of state that incorporates leptonic contributions of arbitrary relativicity and degeneracy (for further details of the convective theory and a discussion of the radiative and conductive opacities, see WZW). Modifications of convective transport and opacities owing to the possible presence of a strong magnetic field were not considered in these calculations. Two-dimensional effects such as magnetically focused accretion are discussed elsewhere (Woosley and Wallace 1981). Our calculations here are strictly applicable only to slowly rotating neutron stars with weak fields, undergoing spherically symmetric mass accretion.

A 1.41 $M_\odot$ neutron star with a radius of 14.3 km was employed for all calculations. These characteristics correspond to a rather "stiff" nuclear equation of state intermediate to those of Bethe and Johnson (1974) and Pandharipande and Smith (1975ab). See Baym and Pethick (1979) for a comparison of R vs. M for various nuclear equations of state. In the present work the neutron star participates only by providing the (nearly constant) gravitational potential in which the explosion occurs.

Thus the only relevant quantity is M/R^2. In all cases we shall be considering events at densities much less than 10^9 g cm^{-3}. This places us in the outer 10^{-8} of the neutron star mass in a region less than 200 m thick composed of "normal" nuclei.

General and special relativistic corrections were not incorporated into the present study. In most cases, such corrections are estimated to be small (Joss and Li 1980), and could be compensated for by small changes in model parameters $(M,R,\dot{M},Z)$ that are inherently uncertain. An exception occurs in the relativistic shock wave produced at the surface of the neutron star by Model C (see Section II), and it is suggested that future calculations of detonating models be carried out to examine the details of this shock wave breakout.

b) Pre-Explosive Models

Taam (1980a) has shown that for a neutron star of given mass and radius there exists a critical accretion rate below which hydrogen will burn in steady state. This is certainly true for cases in which the temperature is high enough to assure β-limitation of the CNO cycle but not high enough to ignite helium burning, and may also be true for lower temperatures. In this steady state, hydrogen consumption proceeds at a rate matching that of surface accretion. A layer of helium accumulates beneath the stably burning hydrogen shell until a sufficient density is attained for helium ignition either by the resonant triple-α reaction (relatively high temperatures) or by pycnonuclear helium burning reac-

tions (very low temperatures).

The thermal history of the neutron star prior to the thermonuclear outburst is an important unknown parameter (Taam 1980ab). We find that only a small fraction, < 0.1%, of the energy from the thermonuclear bursts is conducted into the inner neutron core ($\rho > 10^9$ g cm^{-3}). Since our models produce less than about 10^{42} ergs in the thermonuclear outburst and the thermal content of the neutron star is expected to be ~ 10^{46} ergs (Hansen and Van Horn 1975), the flashes should have a negligible effect on the thermal content of the stellar interior. It is assumed that over the course of many such flashes the neutron core reaches a steady temperature owing to the balance of heat flow inwards from the stable hydrogen burning shell and neutrino losses in the central regions. The temperature of the entire neutron star is thus taken to be that of the hydrogen burning shell. Energy deposited by accretion is presumed to be immediately radiated away without greatly affecting the internal thermal balance.

Since the energy generation rate for the β-limited CNO cycle depends directly on the metallicity, Z, of the material (Hoyle and Fowler 1965), the structure of the hydrogen burning shell is very sensitive to composition. Unfortunately the metallicity is uncertain owing to the possible depletion of the C, N, and O nuclei that may occur in the accreted material because of gravitational settling. Heavy ion depletion has been shown to be important in white dwarf envelopes (Fontaine and Michaud 1979; Alcock and Illarionov 1980). While the diffusion coefficients for the degenerate conditions in the neutron star

envelope are currently too uncertain to calculate the actual metal abundances, we expect the effects to be large, given the substantially higher surface gravity of a neutron star compared to a white dwarf. Because of this uncertainty, as well as the possibility of accreting material from an extreme Population II companion, we have considered both models in which the accreted matter has solar metallicity and various low values of metallicity. Later in Section III we will present a semi-analytic procedure for estimating the outcome of accretion with values of metallicity other than the three representative models discussed here.

The accretion rates used in this study (10^{-11} to 10^{-9} $M_\odot$/yr) may be reasonable for a bare neutron star passing through a dense interstellar cloud, a neutron star in a widely separated binary system with a giant star, or a neutron star in a close binary system dominated by gravitational radiation, such as in some cataclismic variables (Faulkner 1971; Whyte and Eggleton 1980). In fact, Whyte and Eggleton suggest that evolutionary constraints on some cataclismic binaries inherently produce just such accretion rates as considered here (although their calculations were performed specifically in the case of a white dwarf companion, rather than a neutron star).

i) Model A

A 1.41 $M_\odot$ star envelope of 10^{25} g was divided into 80 mass zones, with zones concentrated near the surface. The radius of each zone was

chosen in such a manner as to put the entire star in an initial state of hydrostatic equilibrium. The composition of the "accreted" matter was X = 0.70, Y = 0.2991, and Z = 9×10^{-4}, where X, Y, and Z denote mass fractions of ^{1}H, ^{4}He and metals respectively. Here "metals" were taken to be in the form of $^{14,15}O$ and ^{14}N, since the normal and β-limited CNO cycles are presumed to operate while the material is heated to our initial starting temperature, and such processes concentrate material in those isotopes. This accreted material is presumed to rest on a substrate of pure ^{56}Fe.

For a given neutron star mass, radius, accretion rate $\dot{M}$, and metallicity Z there is a unique steady state temperature T_H, density ρ_H, and accreted mass M_H characterizing the base of a stably burning hydrogen envelope (Hansen and Van Horn 1975, Taam and Picklum 1978). Alternatively, one can take the approach followed here of specifying for a given neutron star the values of Z and T_H, and then calculating the corresponding M_H needed for stable burning. For $T_H = 1.21\times10^{8}$ K and $Z = 9\times10^{-4}$, the stable hydrogen burning layer contained 6.0×10^{21} g. The density at the base of this layer was $\rho_H = 4.28\times10^{5}$ g cm^{-3} and the nuclear contribution to its steady luminosity L_s from the β-limited CNO cycle was 3.1×10^{34} erg s^{-1} (accretion would yield 1.0×10^{36} erg s^{-1} from gravitational energy). Since, in steady state, hydrogen burns at the same rate as material accretes, the nuclear luminosity is just

$$L_s = q_H \dot{M} \quad \text{erg s}^{-1}, \tag{1}$$

where q_H is the energy released from hydrogen burning ($q_H/X = 6.83\times10^{18}$

erg g^{-1}). Thus, the steady state (nuclear) luminosity corresponding to accretion of matter containing 70% hydrogen is

$$L_s \approx 2.66\times10^{34}\ \dot{M}/(10^{-10}\ M_\odot\ yr^{-1})\ \ erg\ s^{-1}, \qquad (2)$$

and the value found above for Model A yields $\dot{M} = 1.2\times10^{-10}\ M_\odot/yr$.

After obtaining the steady state hydrogen burning envelope, the amount of helium beneath the hydrogen shell was increased at a rate equal to the flux of matter through the burning shell (i.e., $\dot{M}$). When the helium layer reached a mass $M_{He} = 1.4\times10^{23}$ g (with a density at its base $\rho_{He} = 6.41\times10^{6}$ g cm^{-3}), a helium runaway ensued.

ii) Model B

Model B was generated from Model A at the point when the helium runaway had just begun, but with the composition of the entire hydrogen envelope switched to pure ^{4}He. This was done in an attempt to circumvent serious numerical difficulties encountered as the helium convective shell penetrated into the hydrogen envelope in Model A (see Section IIc). Elimination of the hydrogen layer once the helium has begun to run away should not have a significant effect on the total gross energetics of the event, as the total nuclear energy available from the hydrogen shell is only about one percent of that available from the helium shell (see also Joss 1978). Also, to facilitate further calculation, the interior of the neutron star in Model B was replaced with a hard inner boundary at R = 14.25 km, $\rho = 2.0\times10^{7}$ g cm^{-3}, with 7×10^{23} g

outside the boundary. The energy flux through the inner boundary was set to zero. Throughout the evolution of Model B the temperature of this inner boundary never rose more than 10% and the artificial removal of the neutron core should have little impact on our results.

iii) Model C

Model C was also generated from a 1.41 $M_\odot$ neutron star in the same manner as Model A, but with an envelope composition of X = 0.70, Y = 0.29996, and Z = 4×10^{-5}. The steady state hydrogen burning solution was characterized by $M_H = 2.4\times10^{22}$ g, $\rho_H = 1.14\times10^{6}$ g cm^{-1}, $T_H = 7.45\times10^{7}$ K, and $L_s = 5.50\times10^{33}$ erg s^{-1}, so that $\dot{M} = 2.07\times10^{-11}$ $M_\odot$/yr. Calculating the evolution as for Model A, we found that a thermonuclear runaway occurred in the helium when $M_{He} = 1.0\times10^{25}$ g and $\rho_{He} = 1.15\times10^{8}$ g cm^{-3}. The interior of the neutron star was replaced with a hard inner boundary at R = 13.444 km, $\rho = 4\times10^{11}$ g cm^{-3}, with 5.5×10^{29} g of material outside the boundary.

iv) Model D

Model D was also generated from a 1.41 $M_\odot$ neutron star in the same manner as Model A, but with an envelope composition of X = 0.70, Y = 0.28, and Z = 0.02 (approximately solar metallicity). The stable hydrogen burning shell was characterized by $M_H = 8.0\times10^{20}$ g, $\rho_H = 1.0\times10^{5}$ g cm^{-3}, $T_H = 1.22\times10^{8}$ K, and $L_s = 9.39\times10^{34}$ erg s^{-1}, so that

$\dot{M} = 3.53 \times 10^{-10}$ $M_\odot$/yr. Calculating the evolution as for Model A, we found that a thermonuclear runaway occurred in the helium when $M_{He} = 2.7 \times 10^{23}$ g and $\rho_{He} = 9.5 \times 10^{6}$ g cm^{-3}. The thermodynamic conditions at the helium shell base in Model D are almost the same as those for Model B, therefore the resulting outburst for the two models should be nearly identical (see Section III). The calculation of Model D was thus terminated at the onset of the runaway, and was performed only to illustrate that an event such as the one calculated for Model B can be produced over a large range in envelope metallicities, with small corresponding changes in $\dot{M}$. Thus for most observational purposes, Model B could also be thought of as a neutron star accreting solar metallicity material at 3.5×10^{-10} $M_\odot$/yr. The characteristics of each model are summarized in Table 1.

c) The Explosive Outburst

i) Model A

The helium runaway in Model A developed on a rapidly accelerating timescale. A time of 10^{6} s was required for the temperature at the helium shell base to rise from 1.2×10^{8} K to 1.3×10^{8} K, an additional 600 s to rise to 1.5×10^{8} K, and only another 10 s to reach 1.9×10^{8} K. Within 0.4 s after attaining 1.9×10^{8} K, the luminosity at the base of the helium layer increased from 4×10^{37} to 7×10^{42} erg s^{-1} and its temperature reached 1.9×10^{9} K. The carbon abundance throughout the helium

convective shell became 19% by mass. During this time, the surface luminosity did not change from its initial value, although a convective zone grew from the base of the helium layer to the hydrogen shell. At the time of convective interpenetration, the temperature at the interface was about 5×10^8 K. As protons were convected into the single helium zone just below the interface, carbon in that zone, which had been produced by prior helium burning, immediately reacted through $^{12}C(p,\gamma)^{13}N(p,\gamma)^{14}O$ causing the energy generation in the zone to increase, within ~ 0.1 μs, from 2×10^{18} erg $g^{-1}s^{-1}$ to 3.5×10^{24} erg $g^{-1}s^{-1}$. By a time of 0.24 μs (15 timesteps) after interpenetration, heat released by proton capture had lowered the temperature gradient in the outer zone of the "helium shell" to a subadiabatic value, ending the convective linkage. At this point the outermost helium zone has changes its identity and becomes the innermost zone in the hydrogen burning shell. Because of the energy input by proton capture on carbon the (new) base of the hydrogen shell becomes convective. During the next 3 μs (30 timesteps), all ^{12}C in this 1.0×10^{21} g zone was depleted, and the mass fraction of ^1H increased from zero to 0.51. Within 7.3 μs after interpenetration, the excess luminosity produced by the flash caused the radius of the photosphere R_p to increase 17 m to R_{max} = 14,330 km. After reaching this radius, the photosphere fell back again, and the surface luminosity increased owing to a combination of compressional heating and convective and conductive transport of energy to the surface from the helium burning shell. The surface luminosity increased from 10^{36} erg s^{-1} to 3×10^{38} erg s^{-1}, and T_{eff} increased from 5×10^6 to 21.3×10^6 K in 0.48 μs.

The thermodynamic structure of the envelope when $L = 1.8 \times 10^{38}$ erg s^{-1} (5 μs after the photosphere reached R_{max}) is shown in Figure 1a. Figure 1b shows the composition of the envelope at this time. A total of 5.47 μs after the photosphere reached R_{max}, it had decreased to a minimum at 14.318 km, and then continued to oscillate several times with a period of about 12 μs before being damped. It is interesting to speculate that if the neutron star contained a strong frozen-in magnetic field (~ 10^{12} gauss may be expected), an impulse of sufficient strength to raise the surface 17 m in 7 μs might produce non-thermal radiation by interacting with the magnetic field (Ramaty et al. 1980).

At a time 275 μs after the first convective shell mixing, the hydrogen and helium shells linked once more, this time raising the photosphere 53 m to 14.385 km in 12.9 μs. An additional 83.7 μs later, a third linking occurred. The small timesteps (~ 10^{-10} s) required to calculate the evolution through the hydrogen/helium convective linkages with realistic mass zoning would require a prohibitive amount of computer time, so the calculation was terminated after the third linking. A total of 2×10^{21} g (~ 30% of the initial envelope abundance) of hydrogen had been consumed by the end of the third linking. The relatively coarse zoning that we employed, combined with the mixing of a single (entire) zone during each convective linkage, introduces considerable uncertainty in our quantitive results for this phenomenon. Temperatures of 8×10^{8} K in the convective zones during linkages suggest that the rp-process of hydrogen burning (Wallace and Woosley 1981) may be important. The regions cool quickly (within a few milliseconds), so that little

nuclear processing beyond ^{21}Mg would be expected; however, the thermodynamic conditions are such that α-captures on Ne, Na, and Mg isotopes may begin to affect the evolution (see Wallace and Woosley 1981; Figure 2).

ii) Model B

Fortunately, the entire store of nuclear energy available in the hydrogen shell is only about one percent of that available in the helium layer. Except for effects produced by the coupling of (hydrogen flash induced) surface oscillations with the magnetic field, the gross characteristics of any burst resulting from a helium shell instability should not be significantly altered by ignoring the presence of the hydrogen layer (Joss 1977). Model B was thus constructed from Model A at the point where the helium runaway had just begun, but with the composition of the "hydrogen" envelope switched to pure ^{4}He. The point at which the energy generation rate exceeded 5×10^{20} erg g^{-1} s^{-1} and the timescale for increasing the temperature 5% declined to under 10 μs was defined as the "onset" of the runaway (t=0). Within the following 1.5 ms, convection transported energy to the surface, producing a luminosity of 10^{38} erg s^{-1}. Thermodynamic conditions in the envelope at this point are shown in Figure 2a. A peak temperature of 3.2×10^{9} K was reached at the base of the helium burning shell, and the surface velocity approached 30 km s^{-1}, although hydrostatic equilibrium was maintained throughout the event. The envelope composition at the same time is shown in Figure 2b.

The convective nature of the deflagration wave smooths the abundances over a large portion of the envelope. By 10 ms about 90% of the helium is consumed, producing ^{56}Ni through a chain of alpha-captures on ^{12}C, accelerated by the ^{12}C + ^{12}C reaction. The temperature sensitivity of these α-capture and carbon burning reactions allow helium to be consumed rapidly enough to produce the high luminosity and rapid rise time of the event. After 10 ms, the ^{12}C abundance has decreased to such a low value that the remaining helium must be burned by the slower, temperature insensitive (at these high temperatures, $\sim 3 \times 10^9$ K) triple alpha (3α) reaction, so that the helium abundance remains above 1% until a time of about 50 s, well after the envelope had become convective. The occurrence of nuclear burning simultaneously with convection may lead to interesting effects (Ruderman 1981), but we have not considered the non-standard modifications to time dependent convection theory that would be required to follow them. Beyond about 50 s, the major energy production mechanism in the model is gravitational contraction rather than nuclear reactions. The light curve for this event is shown in Figure 3a, and the evolution of the photospheric radius and effective temperature is shown in Figure 3b. The rapid rise time (< 3 ms) for the luminosity is given in the inset to Figure 3a. Note, however, that the rise time for this 1D model is even shorter than the sound transit time around the star, and must not be taken as the observable rise time. The runaway would actually be expected to begin at a point, and then propagate along the envelope base at a speed well below sound speed. Two dimensional aspects of thin shell burning in this context are discussed by Ruderman (1981), Woosley and Wallace (1981) and by Fryxell and Woosley (1981, 1982). The

radius did not change significantly until after t = 4 ms, but by t = 15 ms, a combination of increased internal energy and strong radiation pressure (with accompanying mass loss) had increased the effective photospheric radius to a value of 30 km. The luminosity remained constant at the Eddington value (L_{Ed}) for 250 seconds, and then declined rapidly to a value of 0.5 L_{Ed} in about 50 seconds. Figure 4 shows the luminosity at the base of the photosphere (r = 14.35 km), which is over two times L_{Ed}, indicating the large amount of energy being stored in the gravitational potential of the expanding photosphere.

Unfortunately, the Lagrangian nature of our hydrodynamic code prevents a precise tracking of the photospheric evolution past this point. Very tenuous surface zones ($< 10^{14}$ g), which are required to adequately resolve the photosphere, are accelerated to such high velocities ($v \geq v_{esc} \sim c/3$) that the density decreases rapidly in those zones. Although the code is capable of continuous automatic rezoning, following small zones as they move down the steep density gradient separating the neutron star "surface" from the photosphere would require timesteps smaller than 10^{-5} s throughout the 250 s duration of the mass loss phase. The surface zones were therefore limited to $M \geq 10^{19}$ g for reasons of expediency in a "first pass" calculation, even though the photosphere could not be resolved with such coarse zoning. After the luminosity dropped below the Eddington value, the photosphere again receded to the radius of the original neutron star. The final cooling curve, due simply to radiative cooling, could then be obtained.

To dete ne .e mass loss phase might have a steady state solution and to ; ep esolve the photosphere, we picked up the calculation at three r tative points during the "super-Eddington" portion of the evolutio cated in Figure 3a), and zoned the outer layers of the star on a ne scale (down to 10^{14} g per zone). The timestep quickly dr ppe out 1 μs as the apparent radius of the photosphere increased n r e to the fine mass zoning. Once the transient response t tosphere to the abrupt rezoning had passed, the rapid (artifici) se in radius slowed, but the radius continued to expand p lu approximately linearly with time, as shown in Figure 5. This r increase is a result of additional mass being pushed into the e photosphere by a super-Eddington luminosity below. It is importa note that the photosphere is not fixed in Lagrangian coordinate ss flows thr ugh a standing, dynamic photosphere.

If L_d at the photosphere, then the excess energy is abruptly converte n increase in $\dot{m}$ beneath the photosphere, so that the luminosity s near the Eddington value regardless of photospheric location. ore, the effective emission temperature at any time is dete y the radius. Since $\sigma T_{eff}^4 = L/4\pi R_p^2$ with only a lower limit to L in our calculation, this implies an upper limit for T_{eff} (see igure 3b). A more detailed study of the photospheric behavior will require either analytic calculation beyond the scope of the present paper, or the use of an Eulerian hydrodynamic code. Since the mesh in such a code would not expand with the wind particles, this would eliminate the artificial timestep constraint imposed by the Lagrangian

method. However, the qualitative nature of the solution is expected to remain as follows. After a short (few ms) spike of higher $T_{eff} \sim 15 \times 10^6$ K, limited by the inertial response time of the neutron star surface, the photosphere is quickly driven outward by radiation pressure, lowering its effective temperature. The emission temperature T_{eff} then rises very slowly, eventually increasing to a peak as L becomes slightly lower than L_{Ed} and the radius begins to decrease. The radius cannot decrease beyond the value of the initial neutron star, so late in the evolution T_{eff} declines with the decreasing luminosity. Throughout the event, the effective temperature remains quite small ($kT \leq 2$ keV).

In addition to causing the photosphere to expand, the radiation pressure accompanying the super Eddington luminosity also accelerates a small amount of surface material to the escape velocity. Beyond about 20 km, the mass loss rate $\dot{m}_L$ ($\sim 4\pi\rho v r^2$) is <u>almost</u> constant at $\dot{m}_L \sim 10^{18}$ g s^{-1} (Figure 6), but declines slowly at greater distances. This mass loss rate, as measured at infinity, remains within the range (0.7 to 1.5) x 10^{18} g s^{-1} throughout the Eddington limited phase. A total of 2 x 10^{20} g with energy around 100 MeV/nucleon is lost in the radiatively driven wind during the outburst in Model B. Implications of this radiatively driven mass loss are discussed further in Section IV.

(4) <u>Model C</u>

Model C represents a neutron star accreting lower metallicity ($Z = 4 \times 10^{-5}$) material (or more likely, material in which substantial deple-

tion of heavy ions occurs by diffusion following accretion) and at a lower accretion rate ($\dot{M} = 2\times10^{-11}$ $M_\odot$/yr) than Model B. These conditions result in a lower temperature for the burning shells, allowing a larger mass of helium to accumulate, thus producing a more violent runaway, sufficiently violent, in fact, to occur as a detonation wave. Nuclear energy generation behind this wave is produced first by burning helium to form ^{12}C, and then becomes dominated by the reactions $^{12}C + {}^{12}C$ and $^{12}C(\alpha,\gamma)^{16}O$. A chain of alpha captures extending to ^{56}Ni eventually processes all the helium into nickel, although $\lesssim$ 43% of the initial helium in the envelope burns in the detonation wave itself (Figure 7). As it nears the surface, the detonation wave steepens into a strong relativistic shock in the steep density gradient. The shock speed is greater than 0.1c and creates an overpressure $P_2/P_1 > 1000$ in a layer 10^{20} g below the surface. As the shock wave breaks through the surface (about 7 μs after helium ignition), the luminosity rises briefly to 10^{42} erg s^{-1} for a period that lasted only 0.1 μs. Our treatment of this phase is somewhat inaccurate owing to the neglect of special relativity. A very small fraction of the total energy in the event was emitted in this γ-ray "precursor", whose effective temperature reached 1.6×10^8 K. The surface luminosity quickly drops back to 10^{36} erg s^{-1} and remains at approximately that level until the energy deposited in the surface layer by the shock has been released as the envelope settled back onto the star. Heating from the envelope falling back to the surface causes the luminosity to reach the Eddington value about 1 ms after the shock had emerged. Note that this rise time is much faster than the time for radiation to diffuse upwards from the burning shell.

Thermodynamic conditions in the envelope at a time just after the shock reached the surface are shown in Figure 7a. Temperatures as high as 6×10^9 K were reached at the base of the helium shell, and surface velocities exceeding 10^{10} cm s^{-1} were produced. The envelope composition at this time is shown in Figure 7b. Even more than in Model B, the high temperatures produce a nuclear statistical equilibrium that favors free alpha particles until cooling begins. The helium eventually (after the temperature begins to fall) burns completely to ^{56}Ni, which later captures electrons to form ^{56}Fe. Both effects produce an enduring source of nuclear energy. At a time about 2000 s after the beginning of the outburst, the helium abundance has declined to 1%, and the major energy source becomes gravitational contraction, supplemented by ^{56}Ni decay, rather than nuclear fusion. Radius and temperature at the boundary of several representative mass regions in the envelope during the rise in surface luminosity are given in Figures 8a and 8b. Rapid envelope oscillations caused by overshooting equilibrium values may be relevant to the microstructure observed in some γ-ray bursts, if such events are caused by the magnetic confinement of plasma produced by a thermonuclear runaway (see Woosley and Wallace 1981).

The light curve produced by Model C is shown in Figure 9a, and the evolution of the photospheric radius and effective temperature are given in Figure 9b. The dashed line in Figure 9a indicates a typical value for the Eddington luminosity during the first 5500 s. During this time, further processing of hydrogen and helium into ^{56}Ni leads to a small decrease in the opacity near the surface, causing the photospheric lumi-

nosity to increase slightly (see Section IIIc, eq. [17]). Data points in Figure 9a come from finely zoned models and suggest that the variation in the luminosity within the first 1.5 hours is less than about 25%. Figure 9b shows the characteristic hardening of the effective temperature during the burst, followed by softening in the tail. As in Model B, radiatively driven expansion of the photosphere limits kT_{eff} to a few keV. The effective temperature during the precursor spike cased by shock wave breakout is shown in the insert of Figure 9b. Since the radius did not change significantly until well after the shock had broken through the surface, the shape of the luminosity curve during the spike precisely follows that of the T_{eff} curve. The radiation pressure again causes a mass loss, with $\dot{m}_L \sim 10^{18}$ g s^{-1}, during the Eddington luminosity phase, ejecting a total mass of 5×10^{21} g as a radiatively driven wind.

Figure 10 shows the neutrino luminosity L_ν during the outburst. Although a total energy of 1.66×10^{43} ergs was liberated in the event, 89% of this energy is emitted as neutrinos, with only 1.9×10^{42} ergs emitted in photons. The early plateau evident in the neutrino loss curve arises from a balance in power between the neutrino loss rate and the nuclear energy generation rate. Beyond a time of about 6000 s, the neutrino contribution from $^{56}Ni(e^-\nu)^{56}$ is comparable to that from plasma processes. Since the ^{56}Ni decay rate is somewhat uncertain under the thermodynamic conditions prevalent here ($T_9 < 2$), the curve in Figure 10 is dashed beyond 6000 s. For $t > 10^4$ s, ^{56}Ni decay is the dominant neutrino production mechanism.

III ANALYTIC APPROXIMATIONS

a) Stable Hydrogen Burning Shell

The numerical models discussed in Section II suggest that a range of qualitative results (event timescales, deflagration/detonation burning, event energy, etc.) can be produced for various values of mass accretion rate and metallicity. Simple analytic models of the envelope evolution are helpful in illustrating the dominant physical principles involved, and may allow the generalization of numerical models to arbitrary values of $\dot{M}$ and Z. Conditions at the base of a stable hydrogen shell could be determined by detailed integration of the stellar structure equations (Hansen and Van Horn 1975; Taam and Picklum 1979, Taam 1980b), but we chose for simplicity and illustration a semi-analytic method that approximates the hydrogen shell conditions with reasonable accuracy.

If the hydrogen in the accreted matter is to burn at the same rate at which it is accreted, then the nuclear contribution to the luminosity must be given by equation (1). For our chosen parameters, nuclear energy will be generated by the β-limited CNO cycle, with energy supplied at a rate $L_\beta = \varepsilon_\beta M_\beta$. Here ε_β is the energy generation rate (Hoyle and Fowler 1965; Wallace and Woosley 1981) and M_β is the mass of hydrogen that is burning:

$$L_\beta = 5.861 \times 10^{15}\ Z\ M_\beta \quad \text{erg s}^{-1}. \tag{3}$$

Equations (1) and (3), we find the mass in the hydrogen burning shell

$$M_\beta = 6.48\times10^{18}\ X\ (\dot{M}/10^{-10}M_\odot\ yr^{-1})/Z\ \ g\ , \tag{4}$$

where X is the mass fraction of hydrogen and Z, the metallicity of the accreted material.

Using the stellar structure equations for the temperature gradient in radiation transport dominated by conduction) and mass conservation (Clayton 1968) gives the temperature gradient in Lagrangian (mass) coordinates

$$\frac{d(T^4)}{dM} = -3\ \frac{\kappa(r)L(r)}{16\pi^2 acr^4}. \tag{5}$$

While the neutron star has a radius of $R_* = 14.3$ km, the hydrogen shell extends only 20 m down from the photospheric surface, so to good approximation the radius in equation (5), prior to the explosive outburst, may be taken as constant, i.e., $r = R_*$. In addition, we assume $L(r)$ is approximately constant throughout the shell with a value, L_s, given by equation (2). Although this is not strictly true at the base of the shell where most of the nuclear burning is occurring, it is a fairly good approximation for much of the mass of the shell, and is sufficient to obtain a rough estimate for the shell parameters. Integrating equation (5) from the surface ($M = 0$, $T = T_0$) down through an envelope mass M, we obtain

$$T^4 - T_o^4 = \frac{3\bar{\kappa} L_s}{16\pi^2 acR_*^4} M \quad , \tag{6}$$

where $\bar{\kappa}$ is the mass averaged opacity

$$\bar{\kappa} = \frac{\int_o^M \kappa(M)dM}{M} \quad cm^2 g^{-1} \quad . \tag{7}$$

Evaluating equation (6) at the base of the hydrogen layer using equations (1) and (4) gives

$$(T_B^4 - T_o^4)^{1/4} \approx 3.95 \times 10^7 \left[\frac{14.3 \text{ km}}{R_*}\right] \left[\frac{X}{0.7}\left(\frac{\dot{M}}{10^{-10} M_\odot yr^{-1}}\right)\right]^{1/2} \left[\frac{1}{Z}\frac{M_T}{M_\beta}\right]^{1/4} K, \tag{8}$$

where M_T is the total mass of accreted material. To within an accuracy of about 5%, $M_\beta/M_T \sim 0.95$ in all numerical models.

Since the mass and depth of the accreted layer is negligible compared to the neutron star mass and radius, m and r can be assumed to be the constant values M_* and R_*. The equation for mass conservation and the condition of hydrostatic equilibrium then give

$$\frac{dP}{dM} = -\frac{GM_*}{4\pi R_*^4} = \text{constant} \quad . \tag{9}$$

Integrating from the surface (where $P \sim 0$) inward to mass M (in units of g) yields

$$P(M) = 3.56\ M \left(\frac{M_*}{1.41 M_\odot}\right)\left(\frac{14.3\text{km}}{R_*}\right)^4 \text{ dynes cm}^{-2} . \qquad (10)$$

Given $\dot{M}$ and the composition of the accreted material, one can then estimate the mass of the hydrogen layer from equation (4) and the pressure at the base of the layer (we assume $M_\beta/M_T = 0.95$) from equation (10). With a reasonable guess for T_o (to which the equations are very insensitive for $T_o < 10^7$ K) and $\bar{\kappa}$, the temperature at the base of the burning shell can be found from equation (8). The temperature and pressure are then used to obtain the density at the shell base. Opacity here is dominated by electron scattering, but is not necessarily constant because of degeneracy effects. We therefore use an initial guess for $\bar{\kappa}$ to obtain T_H, then determine a grid of κ through the envelope from the temperature (eq. [6]) and pressure (eq. [10]) at each point. Equation (7) is evaluated numerically to obtain $\bar{\kappa}$, and an iteration is performed until a converged value of T_H is found.

The resulting conditions at the base of the hydrogen burning layer for several different metallicities are shown in Figure 11. The curves stop on the left side of the diagram at $\dot{M}_\beta$ where the CNO cycle ceases to be β limited. For $\dot{M} < \dot{M}_\beta$, hydrogen burning reactions regain their temperature sensitivity and may or may not be stable. If a runaway commences, however, the shell may heat up until β limitation again removes the temperature sensitivity. If the conditions are such that helium burning is initiated in the hydrogen helium layer prior to the onset of the β limited cycle, then a combined hydrogen helium runaway will occur (Taam 1980bc). There also exists a critical accretion rate $\dot{M}_c$ such that

for $\dot{M} > \dot{M}_c$, helium burning begins prior to hydrogen depletion. In such cases the high temperature sensitivity of the triple-alpha reaction combined with hydrogen burning by the rp-process (Wallace and Woosley 1981) results in a thermally unstable hydrogen shell (Taam 1980bc). This critical accretion rate depends on Z but may be as high as 10^{-9} $M_\odot$/yr for Z = 0.02 or as low as 10^{-10} $M_\odot$/yr for $Z = 4 \times 10^{-4}$ (Taam 1980c). Thus Figure 11 should not be used when $\dot{M} > \dot{M}_c$. The data points in Figure 11 represent the stable hydrogen envelopes for Models A/B, C, and D. Our results also agree very well with the numerical envelope integrations done by Taam (1980c). The inverse dependence of $T(\dot{M})$ upon Z (eq. [8]) accounts for the flattening of the curves in Figure 11 at higher Z.

b) Helium Ignition

Once the parameters of the stable hydrogen shell have been determined from Figure 11, a rough estimate for the density at the base of the helium shell at the time it reaches a critical mass can be found by comparing the radiation diffusion timescale, τ_R, with the nuclear heating timescale $\tau_{3\alpha}$. Each timescale is $\tau = RT/\epsilon$, where R is the universal gas constant, T is the temperature, and ϵ is the energy generation or loss rate in erg g^{-1} s^{-1}. For Helium burning,

$$\tau_{3\alpha} = 9.647 \times 10^{17} Q_{eff}(\mathrm{MeV}) dY/dt \quad \mathrm{erg\ g^{-1}\ s^{-1}}, \tag{11}$$

where Q_{eff} is the effective Q value for the reaction $3\alpha \rightarrow \frac{3}{11}(^{12}C) + \frac{6}{11}(^{16}O)$, since in steady state the triple alpha reaction

is occasionally followed by $^{12}C(\alpha,\gamma)^{16}O$, producing a ratio of ^{16}O to ^{12}C of roughly 2 to 1. Here dY/dt is the rate of change of the ^4He mass fraction. Thus,

$$\varepsilon_{3\alpha} \approx 2.477\times10^{16}\rho^2Y^3f_s\lambda_{3\alpha} \quad \text{erg g}^{-1}\text{s}^{-1}, \tag{12}$$

where f_s is the electron screening correction factor discussed in the Appendix and $\lambda_{3\alpha}$ is the triple-alpha reaction rate (not divided by 6) of Fowler , Caughlan, and Zimmerman (1975). A thermal diffusion energy loss rate can be defined from the temperature gradient equation as

$$\varepsilon_R = \frac{4ac}{3\kappa} T^4(\rho H_p)^{-2} \quad \text{erg g}^{-1}\text{s}^{-1} \quad , \tag{13}$$

where H_p is a pressure scale height. Again taking $R = R_\odot$ and $M = M_\odot$ as constants,

$$H_p = \frac{PR^2}{\rho GM} \quad \text{cm}. \tag{14}$$

The pressure can be easily estimated since it is due almost entirely to degenerate, relativistic electrons when $\rho > 3.7 \times 10^6$ g cm^{-3} for $Y = 1$. Setting $\tau_{3\alpha} = \tau_R$ gives

$$\rho^{14/3} = \frac{4.321\times10^{14}\ T_9^4}{\kappa f_s\lambda_{3\alpha}} \ , \tag{15}$$

which has been plotted in Figure 12. The curve stops on the left side of the diagram where we expect gross uncertainty in the screening correction. This occurs at the dashed line labelled $b = 1.6$ (see the

Appendix). The curve labelled $\Gamma_{84} = 168$ shows approximately where the liquid/solid phase transition occurs in helium, so that a pycnonuclear triple-alpha reaction rate must be employed. It seems that investigations of lower temperature (i.e., lower $\dot{M}$ and lower Z than treated here) models must await the development of a more comprehensive treatment of electron screening and pycnonuclear reactions. The total mass of the envelope, also indicated in Figure 12, can be found by solving equation (10) using the degenerate electron equation of state and assuming most of the envelope mass is in helium. The data points plotted in Figure 12 show the conditions present in the numerical models when thermal instabilities developed.

c) Radiation Driven Wind and the Photosphere

Both Models B and C experienced a sustained epoch of radiatively driven mass loss during which L remained near the Eddington value and mass was lost at a rate of about 10^{18} g s^{-1}. The Eddington Luminosity is the luminosity at which the pressure required for hydrostatic equilibrium is completely supplied by the radiation flux. If radiation pressure ($P = aT^4/3$) is substituted into equation (11), then

$$\frac{dP}{dr} = \frac{-GMp}{r^2} = \frac{4}{3}aT^3\frac{dT}{dr} \quad . \tag{16}$$

Using the diffusion equation for dT/dr yields the Eddington Luminosity as

$$L_{Ed} \quad 4\pi \qquad \text{erg s}^{-1} \tag{17}$$

$$2 \qquad 38\left(\frac{0.2}{\kappa}\right)\left(\frac{M}{M_\odot}\right) \quad \text{erg s}^{-1} \quad , \tag{18}$$

and for a $M_\odot$ neutron star with $\kappa = 0.34$ (electron scattering), L_{Ed} = 2.1x10 s^{-1}. Both Models B and C show that when a large radiation flu uddenly deposited in the star's outer layers, the photosphere q y (within about one millisecond) expands to where it can radiate bout the Eddington luminosity, with an accompanying radiatively d n wind. This effect suggests that without confining the surface p (e.g., with magnetic fields, as discussed in Woosley and Walla), the surface will always swell to a large radius and radiate ~ 2 keV) x-rays at approximately the Eddington luminosity. How Wilson, and Barton (1981) have found the same Eddington limit (again achieved within 1 ms) in their two-dimensional calculation of a neutron star - asteroid collision. Thus, a hard γ-ray burst from thermal processes is probably not possible without magnetic confinement.

To obtain a semi empirical estimate of the mass loss rate arising from the radiatively driven wind, suppose the luminosity is slightly above L_{Ed}, $L = fL_{Ed}$, where $f \gtrsim 1$. The net force on a spherical shell of mass (i.e., the excess over that required to balance gravity) is (Faulkner 1970)

$$F = \int P_{excess} dA = (f-1)L_{Ed}/c$$

$$= (f-1)4\pi GM/\kappa \quad \text{erg cm}^{-1} \quad . \tag{19}$$

The amount of mass accelerated to the escape velocity, v_{esc}, in time t is m, where

$$v_{esc} \approx (F/m)t$$

$$= \frac{(f-1)L_{Ed}t}{mc} \quad \text{cm s}^{-1} \quad . \tag{20}$$

Since m/t is approximately the mass loss rate $\dot{m}$ (= dm/dt), we have

$$\dot{m} \approx \frac{(f-1)L_{Ed}}{v_{esc}c} \quad \text{g s}^{-1} \quad , \tag{21}$$

where $v_{esc} = (2GM_*/R)^{1/2}$ cm s^{-1}. For a 1.41 $M_\odot$ star with R = 14.3 km, r = 0.2, and f = 2, equation (21) gives $\dot{m} \sim 8\text{x}10^{17}$ g s^{-1}, comparable to the values found in our model calculations.

As discussed in Section II, our Lagrangian hydrodynamic code is unable to follow the detailed evolution of the expanding photosphere; however, an analytic upper limit on the photospheric radius R may be obtained. The mass loss rate

$$\dot{m} = 4\pi r^2 \rho v \tag{22}$$

is constant for sufficiently large r. Assuming $v \propto r^n$ in the region of interest, with $n > 0$ and approximately constant, then the density is given by

$$\rho(r) = \rho(R)(R/r)^{n+2} \quad \text{g cm}^{-3} \quad , \tag{23}$$

where R is a radius at which the density $\rho(R)$ is known. Substituting equation (23) into the definition of the photospheric radius R_p,

$$\int_{R_p}^{\infty} \rho\kappa \, dr = /3 \quad , \tag{24}$$

and integrating (with $\kappa \sim$ constant) yields

$$\rho(R_p)R_p = (10/3)(n+1)(0.2/\kappa) \quad g\ cm^{-2}, \tag{25}$$

and $\kappa \sim 0.2$ throughout the photospheric region in the numerical models. Since R_p must be greater than the initial radius of the neutron star, we may conclude that $\rho(R_p) < 10^{-6}$ g cm^{-3}.

In addition $\rho(R_p)$ is limited by the fact that the atmosphere can not contain more material than has been ejected from the neutron star surface since the event began:

$$\int_{r_i}^{R_p} 4\pi r^2 \rho(r) dr < \int_0^t \dot{m} dt = \dot{m}t \quad , \tag{26}$$

where r_i is the injection radius, defined by the distance beyond which $\dot{m}$ is constant. Substituting equation (23) into equation (26) yields

$$4\pi\rho(R_p)R_p^{n+2}\int_{r_i}^{R_p} r^{-n} dr < \dot{m}t \quad . \tag{27}$$

The numerical models suggest $n \sim 1$ near $r \sim R_p$, so

$$4\pi R_p^3 \rho(R_p)\ \ln(R_p/r_i) < \dot{m}t \quad . \tag{28}$$

Substituting equation (25) into equation (28) and using $\kappa = 0.2$, $\dot{m} = 10^{18}$ g s^{-1} gives

$$R_p^2 \ln(R_p/r_i) < 10^{16} t \quad . \tag{29}$$

Thus, for $r_i \sim 18$ km, R_p must be less than 540, 1500, and 4300 km for times of 1, 10, and 100 seconds respectively. Note that these values are gross overestimates, since they were obtained using an unrealistically large mass for the envelope (i.e., assuming that no mass fluxed through the photosphere).

d) Elemental Diffusion

The recurrence timescales (total envelope mass divided by $\dot{m}$) for the numerical models described here range from 4 months to 240 years. This may be long enough for gravitational settling of heavy ions to significantly alter the envelope composition (Rosen 1969), and hence the thermal structure of the entire accreted layer. Unfortunately, reliable estimates for the diffusion coefficients in very degenerate material do not yet exist, although recent estimates of the diffusion timescale in the atmospheres of white dwarfs (Fontaine and Michaud 1979, Alcock and Illarionov 1980) suggest that such a process is very important there. Given the much stronger surface gravity of a neutron star, one might expect gravitational settling of heavy ions to be an important effect in

neutron star atmospheres. According to Fontain and Michaud (1979), the abundance by mass of a trace element 2 diffusing through the major constituent 1 at a depth where the diffusion velocity is w_t is given by

$$X_2 = X_2(0)\exp(-t/\Theta), \tag{30}$$

where the diffusion timescale Θ is given by

$$\Theta = 7.958\times10^{-14}\Delta M(R_6^2\rho w_t)^{-1} \quad s\ , \tag{31}$$

ΔM is the mass in g between this point and the surface, R_6 is the radius in 10^6 cm, and ρ is the density. The diffusion velocity is $w_t = w_g(1+f')$, where w_g is the diffusion velocity due to gravitational settling alone (the pressure gradient term) and f' expresses the relative importance of thermal diffusion to gravitational settling. w_g can be written as

$$w_g = D_{12}[\frac{A_2}{A_1}(1+Z_1)-Z_2-1]\rho g/P \quad , \tag{32}$$

where A_i and Z_i are the atomic weight and charge of species i, g is the gravitational acceleration, and P is the pressure. The diffusion coefficient D_{12} is given by

$$D_{12} = \frac{1.0259\times10^3\ T_7^{5/2}}{\hat{A}^{1/2}\rho(X_1/A_1)Z_1^2Z_2^2A_1(2)} \quad , \tag{33}$$

where T_7 is the temperature in 10^7 K, $\hat{A}=A_1A_2/(A_1+A_2)$ is the reduced

atomic weight, and $A_1(2)$ is the logarithmic term

$$A_1(2) = \ln(1+\chi_D^2), \tag{34}$$

$$\chi_D^2 = \frac{4.530\times10^5\ T_7^3}{Z_1^2 Z_2^2 \rho(\sum_i X_i Z_i^2/A_i)} \quad . \tag{35}$$

At the base of the hydrogen layer in Model C, the conditions listed in Table 1 give $A_1(2) = 1.68$ for the diffusion of ^{12}C through a hydrogen plasma. Fontain and Michaud suggest that their method breaks down (owing to degeneracy effects) for $A_1(2) < 3$ and may underestimate Θ by a factor of 10 when $A_1(2) = 0.1$. Nevertheless, if this value is used to estimate a diffusion timescale the result is $\Theta \sim 1\times10^7$ s (f' depends on dlnT/dlnP and is much less than 1 here). Thus in Model C the metal diffusion timescale is about 4 months while the accretion timescale for the accumulation of the 2.4×10^{22} g hydrogen envelope is about 7 months. Such similar timescales suggest that diffusion effects could be important. However, Alcock and Illarionov (1980) suggest multiplying equation (35) by $\eta^{1/2}\exp(\eta)$, where η is the degeneracy parameter. For Model C, $\eta \sim 33$ at the hydrogen shell base, so Θ would increase a factor of 20. Further effort to determine D_{12} in degenerate situations is obviously needed.

IV. SUMMARY

Type I x-ray bursts, certain fast x-ray transients, and some gamma-ray bursts may all be a family of events resulting from thermonuclear runaways (mainly involving helium) on accreting neutron stars (γ-ray bursts will require the presence of a magnetic field and will be discussed in a subsequent paper: Woosley and Wallace 1981). The most important parameters distinguishing these events are the accretion rate $\dot{M}$, the metallicity Z of the accreted material, the magnetic field strength B, and, to a lesser extent, M_*/R_*^2 and the rotation rate. Lower $\dot{M}$ and Z lead to thicker helium layers and therefore produce bursts of greater energy and longer duration.

In extreme cases, degenerate helium ignition may be so violent as to produce a nuclear detonation wave. Accumulation of a sufficiently thick helium layer for a detonation to develop seems a likely consequence of low accretion rates and/or low metallicity (possibly owing to gravitational settling). For even lower values of $\dot{M}$, a hydrogen/helium shell flash may result, rather than the accumulation of a thick helium layer (Taam 1980b). The helium detonation scenario for moderately low $\dot{M}$ and Z may be more plausible than the carbon detonations originally envisioned by Woosley and Taam (1976) because the hydrogen burning shell may be stabilized by beta limitation while a stable low temperature helium burning shell is more difficult to obtain. Also, our helium shells burn directly to ^{56}Ni and produce negligible ^{12}C.

Super-Eddington luminosities from thermonuclear burning on a neutron star surface will promote extensive mass loss in the form of a radiatively driven wind. The mass loss rate will be of the order 10^{18} g s^{-1} and will endure so long as the luminosity exceeds the Eddington value. This extreme radiation pressure causes the photosphere to extend to several times the original neutron star radius within about 10 ms following helium ignition. At this large radius, the [illegible] diates low energy (~ 2 keV) x-rays at a luminosity near the Eddington value. While we have not examined less energetic models (with higher accretion rates) that may make more typical x-ray bursts (e.g., Joss 1978; Taam 1980a), observations of such events indicate $L \sim L_{Ed}$ (e.g., Lewin et al. 1976), so the photosphere in those cases may also not correspond to the radius of a cold neutron star. If so, certain "flat top" Type I x-ray bursts may also be expected to exhibit the soft-hard-soft spectral evolution discussed below for our more energetic events. Indeed, just such an evolution in the spectra of the Terzan 2 x-ray burst has been observed by Grindlay et al. 1980. We also see evidence for such a spectral evolution in the 1979 July 21 and July 24 burst spectra observed by Makishima et al. (1981; their Figure 3). We also note that treatment of the photosphere in previous calculations of x-ray bursters (Joss 1978, Joss and Li 1980) has often been artificial and without the use of extremely fine mass zoning (we employed zoning down to 10^{14} g to study the mass loss), which may have suppressed this important effect.

Material lost from the neutron star is important for a variety of reasons: 1) Since the photosphere no longer corresponds to the surface

of the cold neutron star, spectral considerations (e.g., redshifted lines or L/T_{eff}^4) may not furnish useful information on the equation of state for high density matter. Care should be taken to use such considerations only when the luminosity is known to be substantially sub-Eddington. 2) The ejected material will have a velocity comparable to the escape velocity of the neutron star (about 100 MeV/nucleon). Such energetic particles might cause an observable γ-line signal from nuclear inelastic scattering reactions, especially if trapped in the neutron star magnetosphere. 3) The total amount of energetic particles ejected into the galaxy in this manner could be an important contribution to low energy cosmic rays. 4) A portion of the ejected matter may be trapped in an extended magnetosphere and later re-accreted. This would lead to enduring post event activity from the high energy transient. 5) Near-relativistic electrons are ejected, and if a magnetic field is present, cyclotron radiation might be produced.

The effective temperature for the transients in our study is low (about 10^7 K) during the Eddington Luminosity phase, owing to the size of the extended photosphere. As the luminosity falls slightly below I_{Ed} and the photosphere recedes, T_{eff} rises sharply to a peak (when the radius again reaches that for the initial cold neutron star), then gradually falls off with the decreasing luminosity. This sharp rise followed by a decrease in the effective temperature, as the luminosity declines below the Eddington value, should be characteristic of all Eddington limited x-ray transients.

The two specific model calculations followed to completion and presented here produce fast x-ray transients lasting from about 5 minutes to 2 hours, although we suspect that varying $\dot{M}$ and Z could extend the range significantly in both directions. These time scales are to be compared to models for x-ray bursts studied by Joss and Li (1980), which last only a few seconds. Several x-ray transients with durations ranging from 12 s to a few hours have been observed (Cook 1976; Schrijver et al. 1978). In addition, the fast x-ray transients with precursors described by Hoffmann et al. (1978) have timescale and spectral characteristics that agree well with our models. We fail, however, to produce the precursors (separated by several seconds from the main event) present in those observations.

Several unresolved problems are particularly in need of further study. A quantitative assessment of the role of gravitational settling in depleting the metallicity of accreted matter is required. The steady state hydrogen shell temperature depends explicitly on Z, since the limited energy generation rate is directly proportional to the metallicity. If the hydrogen shell determines the temperature in the helium layer through conduction, then the helium mass, and hence the event energy, depends on Z. Studies of strong and pycnonuclear screening corrections for helium burning are essential for determining the evolution of models with extremely low Z or $\dot{M}$, where "cold" ($\lesssim 6\times10^{7}$ K) helium shells with base densities above 10^{9} g cm^{-3} may be formed. Further 1D calculations of stars with somewhat lower accretion rates (and thus low hydrogen shell temperature) than considered here, and

Eulerian recalculations of the present models to determine more accurate photospheric evolution during the Eddington Luminosity phase, should provide important results. Full 2D calculations are required to determine the propagation characteristics of a detonation or deflagration wave along the neutron star surface, since the ignition would actually [illegible] at a single point ([illegible]). Note that the rise times suggested by the 1D models presented in this paper are significantly shorter than the sound travel time around the star, and must not be taken as observable rise times. In fact, Makishima *et al*. (1981) have recently observed three type I x ray bursts having rise times of 5–10 s, rather than the usual $\lesssim$ 2 s for such events. This relatively long rise time might be consistent with a helium runaway similar to the high $\dot{M}$ accretion cases studied by Joss (e.g., Joss 1978; Joss and Li 1980), but where temporal allowance must be made for the deflagration wave to propagate around the stellar surface.

loss were also helpful. We are grateful for the assistance of B.
a in the preparation of Figure 8. This work was supported in part
s National Science Foundation through grants AST 79-09102 and AST
509, and, at Livermore, by the U. S. Department of Energy through
many
ict number W-7405-ENG-48.
for m
their
covic
tron
the A
sions
mass
Wilso
by th
81-08
contr

The authors wish to express their gratitude to Dr. R. E. Taam for helpful discussions throughout the course of this work, as well as aking available the results of several important studies before publication. Discussions with Dr. H. DeWitt and Professor B. Jani were useful in developing a formalism for calculating the elec-

APPENDIX

ELECTRON SCREENING

The reaction rates used in our numerical calculations have been corrected for the effects of electron screening as described by Graboske et al. (1973). Their formulation, however, evaluates key parameters in the screening function by assuming the interacting nuclei to be at zero separation. More recently, other methods have been developed to take into account the important spatial dependence of the screening function, and we have adapted one such method to calculate the screening enhancement included in the results shown in Figure 12. Itoh et al. (1979) included spatial dependence in their calculation of the enhancement factor for a general mixture of ions by linearly extrapolating DeWitt's (1979) Monte Carlo computation data for the screening function to zero separation. Jancovici (1977) has shown that the spatial dependence is quadratic near the origin, leading to significantly different results from those obtained with a linear extrapolation (DeWitt 1980). Alastuey and Jancovici (1978) have calculated the screening correction factor for a one component plasma using the more accurate quadratic spatial dependence of the screening function. Following the method suggested by Jancovici (1980), we may generalize the results of Alastuey and Jancovici (1978) to an arbitrary mixture of ions. The dimensionless parameter, τ, of Alastuey and Jancovici can be generalized to (e.g., Itoh et al. 1979)

$$\tau_{12} = \left[\left(\frac{27\pi^2}{4}\right)\frac{2\hat{A}Z_1^2Z_2^2e^4}{N_A kTh^2}\right]^{1/3} \tag{A1}$$

$$= 4.24872\left[\frac{Z_1^2Z_2^2\hat{A}_{12}}{T_9}\right]^{1/3} , \tag{A2}$$

where $\hat{A}=A_1A_2/(A_1+A_2)$ is the reduced atomic number, Z_1 and Z_2 are the charges of the two reacting particles, and T_9 is the temperature in units of 10^9 K. Alastuey and Jancovici obtained a screening enhancement factor for the one-component system of $f = \exp H$, where

$$H = C-\frac{\tau}{3}\left(\frac{5}{32}b^3-0.014b^4-0.128b^5\right)-\Gamma\left(0.0055b^4-0.0098b^5+0.0048b^6\right). \tag{A3}$$

C was calculated by Jancovici (1977), $b = 3\Gamma/\tau$, and Γ will be discussed below. The constant C was computed using the result from the Monte Carlo calculations on binary mixtures of Hansen et al. (1977) that the excess free energy F of a mixture of N_1 ions (charge Z_1) and N_2 ions (charge Z_2) obeys

$$\beta F = N_1 f_o(\Gamma' Z_1^{5/3})+N_2 f_o(\Gamma' Z_2^{5/3}) , \tag{A4}$$

where $1/\beta = kT$, $\Gamma' = \beta e^2/a'$, $a' = (3/4\pi n_e)^{1/3}$ and f_o is the excess free energy of the one-component system. If equation (A4) can be generalized to an arbitrary mixture, then C becomes (Mochkovitch 1980, Jancovici 1980)

$$C = f_o(\Gamma' Z_1^{5/3}) + f_o(\Gamma' Z_2^{5/3}) - f_o(\Gamma'(Z_1+Z_2)^{5/3}) \quad , \tag{A5}$$

where the electron number density is

$$n_e = \sum_k n_k Z_k$$

$$= \rho N_A \sum_k Z_k X_k / A_k \quad , \tag{A6}$$

and X_k is the mass fraction of species k. Combining equation (A6) with the definition of Γ' and a' gives

$$\Gamma' = \frac{e^2}{kT}\left[\frac{4\pi n_e}{3}\right]^{1/3}$$

$$= 2.27493 \times 10^{-4} [\rho(\sum_k Z_k X_k / A_k)]^{1/3} / T_9 \quad , \tag{A7}$$

where ρ is the density in g cm $^{-3}$. The Monte Carlo computer results for the excess free energy f_o are fit in the range $0.8 < \Gamma < 168$ by (Hansen et al. 1977)

$$f_o(\Gamma) = -0.896434\Gamma + 3.44740\Gamma^{1/4} - 0.5551 \ln\Gamma - 2.996 \tag{A8}$$

Using equations (A8) and (A7) in equation (A5) yields

$$C = 0.896434\Gamma' \tilde{z} \; 3.44740\Gamma'^{1/4}\tilde{z} - 0.5551(\ln\Gamma' + (5/3)\ln(Z_1 Z_2/(Z_1+Z_2))$$

$$-2.996 \quad , \tag{A9}$$

where

$$\tilde{z} = (z_1+z_2)^{5/3}-z_1^{5/3}-z_2^{5/3}$$

$$\tilde{\tilde{z}} = (z_1+z_2)^{5/12}-z_1^{5/12}-z_2^{5/12}$$

The second term in equation (A3), $(\tau/3)5b^3/32$, is the first term in the expansion near the origin of the potential of mean force, $z_1z_2e^2/r + w(r)$, which is related to the classical pair correlation function $g_c(r)$ by

$$g_c(r) = \exp(-\beta[Z_1Z_2e^2/r+w(r)]) \quad .$$

Jancovici (1977) showed that w(r) can be written as

$$\beta w(r) = -C + \frac{\pi(Ze)^2}{3kT}\frac{n_e}{Z}r^2 + \ldots \qquad (A10)$$

For a multi-component plasma, the definitions of Γ', a', and $\langle Z\rangle = (Z_1+Z_2)/2$ can be used to write equation (A10) as

$$\beta w(r) = -C + \frac{Z_1Z_2}{2(Z_1+Z_2)}\Gamma'\left(\frac{r}{a'}\right)^2 + \ldots \qquad (A11)$$

Expanding equation (A11) in a Taylor Series by the method of Alastuey and Jancovici (1978), and using equation (A1) yields the result for H of

$$H = C - \frac{\tau}{3}\frac{5}{32}\left[\frac{3Z_1Z_2\Gamma'}{\tau_{12}}\left(\frac{Z_1+Z_2}{2}\right)^{1/3}\right]^3 + \ldots \qquad (A12)$$

This can be identified with equation (A3) if $\tau = \tau_{12}$ and $\Gamma = \Gamma_{eff}$, where

$$\Gamma_{eff} = \left(\frac{2}{Z_1+Z_2}\right)^{1/3} Z_1 Z_2 \Gamma' \quad . \tag{A13}$$

The other terms in equation (A3) were obtained by analyzing the computer results for the pair distribution function of a one-component plasma. In the absence of computer results for arbitrary plasmas, we have assumed that the remaining terms in equation (A3) can be generalized as in equation (A12) with the substitution $b = 3\Gamma_{eff}/\tau_{12}$.

In summary, we have computed the screening correction in the strong screening region $0.8 \leq \Gamma_{eff} \leq 168$ by using equation (A3) with equations (A2), (A7), (A9), and (A13). This formalism is only valid in the range $0 \leq b \leq 1.6$ (Alastuey and Jancovici 1978). For weak screening, $\Gamma < 0.3$ (De Witt 1978), the prescription in Graboske et al. was used:

$$H_w = Z_1 Z_2 A^{1/2} (\Sigma Z_k^2 X_k/A_k + \Sigma Z_k X_k/A_k) 1.88 \times 10^8 (\rho/T^3)^{1/2} \quad . \tag{A14}$$

For intermediate screening, $0.3 \leq \Gamma \leq 0.8$ (DeWitt 1978), an average of the weak and strong screening results was used, as suggested by Salpeter and Van Horn (1969):

$$H = \frac{H_w H_s}{(H_w^2 + H_s^2)^{1/2}} \quad . \tag{A15}$$

Finally, we could find no recent screening formalism for helium in the pycnonuclear region of $\Gamma_{eff} > 168$ (DeWitt 1980). Extremely important studies of x- and γ ray burst models at very low temperatures and high

densities await the development of reasonable screening approximations for $b > 1.6$ and $\Gamma_{eff} > 168$.

The screening correction for the triple alpha reaction was computed in the manner suggested by Salpeter and Van Horn (1969) of taking

$$R_{3\alpha} = R(\alpha+\alpha)+R(^{8}Be+\alpha) \quad , \tag{A16}$$

although there has been some recent controversy over the validity of this method (Jancovici 1980).

For the conditions at the helium ignition point shown in Table 1 for Model B, the Graboske et al. (1973) screening factor is 11.56, whereas the above formalism gives 11.68. For the conditions at the corresponding point in Model C, the Graboske et al. factor is 1.42×10^{5}, and the factor from the above formalism is 6.34×10^{4}. Thus, the screening in our numerical calculations is not off by more than about a factor of two in the worst case from that suggested by most recent work, and the results presented should be reliable. However, for the lower temperatures and higher densities appropriate to models with lower values of $\dot{M}$ and Z (see Figures 11 and 12) than treated here, the formalism described in this appendix differs significantly from older methods. For example when $\dot{M} = 10^{-11}$ $M_{\odot}$/yr and $Z = 10^{-5}$ (perhaps owing to diffusion effects), the expected temperature (from Section IIIa) is about 5.6×10^{7} K and the density at the base of the helium layer may be as high as 10^{9} g cm^{-3}. In this case, the Graboske et al. screening factor is 3.8×10^{14} and we would calculate 1.5×10^{12}, a factor of 250 lower.

TABLE 1

NUMERICAL MODEL CHARACTERISTICS

		Model A	Model B	Model C	Model D
$\dot{M}$	($M_\odot$/yr)	1.16 (-10)	1.16 (-10)	2.07 (-11)	3.53 (-10)
Z		9 (-4)	9 (-4)	4 (-5)	2 (-2)
M_H	(g)	6.0 (+21)	————	2.4 (+22)	8.0 (+20)
ρ_H	(g cm^{-3})	4.28 (+5)	————	1.14 (+6)	1.00 (+5)
T_H	(K)	1.21 (+8)	1.21 (+8)	7.45 (+7)	1.22 (+8)
ΔR_H	(m)	1.7 (+1)	————	2.3 (+1)	1.0 (+1)
M_{He}	(g)	1.40 (+23)	1.40 (+23)	1.00 (+25)	2.70 (+23)
ρ_{He}	(g cm^{-3})	6.41 (+6)	6.41 (+6)	1.15 (+8)	9.55 (+6)
ΔR_{He}	(m)	1.5 (+1)	1.5 (+1)	7.3 (+1)	3.6 (+1)
ΔM[a]	(g)	————	2 (+20)	5 (+21)	————
$\dot{m}$[b]	(g/s)	————	1 (+18)	1 (+19)	————
E_γ	(erg)	————	1.28 (+41)	1.90 (+42)	————
E_υ	(erg)	————	3.91 (+38)	1.47 (+43)	————
τ_L[c]	(s)	————	3.20 (+2)	6.50 (+3)	————
τ_{rise}[d]	(ms)	————	1.5	1	————
τ_{rec}	(yr)	6.1 (-1)	6.1 (-1)	2.4 (+2)	3.8 (-1)

[a] Total Mass lost during the outburst.

[b] Mass loss rate during wind phase.

[c] Time during which L > 0.5 L_{Ed}.

[d] Time for L to reach 0.5 L_{Ed}.

REFERENCES

Alastuey, A., and Jancovici, B. 1978, Ap.J., 226, 1034.

Alcock, C., and Illarionov, A. 1980, Ap.J., 235, 534.

Baym, G., and Pethick, C. 1979, Ann. Rev. Astr. Ap., 17, 415.

Beaudet, G., Petrosian, V., and Salpeter, E.E. 1967, Ap.J., 150, 979.

Bethe, H.A., and Johnson, M.B. 1974, Nucl. Phys., A230, 1.

Clayton, D.D. 1968, Principles of Stellar Evolution and Nucleosynthesis (New York: McGraw Hill), pp. 131, 183.

Cooke, B.A. 1976, Nature, 261, 564.

DeWitt, H.E. 1978, Strongly Coupled Plasmas, ed. by G. Kalman and P. Carini (New York: Plenum Pub. Corp.), p.81.

_____ 1979, private communication.

_____ 1980, private communication.

Lewin, W.H.G. et al. 1976, M.N.R.A.S., 177, 83P.

Faulkner, D.J. 1970, Ap.J., 162, 513.

Faulkner, J. 1971, Ap.J., 170, L99.

Fontaine, G., and Michaud, G. 1979, Ap.J., 231, 826.

Fowler, W.A., Caughlan, G.R., and Zimmerman, B.A. 1975, Ann. Rev. Astr. Ap., 13, 69.

Fryxell, B.A., and Woosley, S.E. 1981, Ap. J., in press.

_____ 1982, BAAS, 13, 792, and in preparation for Ap. J.

Fugimoto, M.Y., Hanawa, T., and Miyaji, S. 1980, preprint.

Graboske, H.C., DeWitt, H.E., Grossman, A.S., and Cooper, M.S. 1973, Ap.J., 181, 457.

Grindlay, J.E. et al. 1980, Ap.J. (Letters), 240, L121.

Hansen, J.P., Torrie, G.M., and Vieillefosse, P. 1977, Phys. Rev. A,

16, 2153.

Hansen, C.J., and Van Horn, H.M. 1975, Ap.J., 195, 735.

Hoffman, J.A., Lewin, W.H.G., Doty, J., Jernigan, J.G., Hardy, M., and Richardson, J.A. 1978, Ap.J. (Letters), 221, L57.

Howard, W.M., Wilson, J.R., and Barton, R.T. 1980, preprint.

Hoyle, F., and Fowler, W.A. 1965, in Quasi-Stellar Sources and Gravitational Collapse, ed. I.Robinson, A. Schild, and E.L. Shucking (Chicago: Univ. of Chicago Press), p. 17.

Itoh, N., Totsuji, H., Ichimaru, S., and DeWitt, H.E. 1979, Ap.J., 234, 1079.

Jancovici, B. 1977, J. Stat. Phys., 17, 357.

_____ 1980, private communication.

Joss, P.C. 1977, Nature, 270, 310.

_____ 1978, Ap.J. (Letters), 225, L123.

_____ 1979, Comments Ap., 8, 109.

_____ 1980, Ann. N. Y. Acad. Sci., 336, 479.

_____ 1971, Fundamental Problems in the Theory of Stellar Evolution, ed. D. Sugimoto, D.Q. Lamb, and D.N. Schramm, (D. Reidel: Dordrecht) 207.

Joss, P.C., and Li, F.K. 1980, Ap.J., 238, 287.

Lamb, D.Q., and Lamb, F.K. 1978, Ap.J., 220, 291.

Lewin, W.H.G., and Clark, G.W. 1980, Ann. N. Y. Acad. Sci., 336, 451.

Makishima, K. et al. 1981, Ap.J. (Letters), 244, L79.

Maraschi, L., and Cavaliere, A. 1977, Highlights of Astronomy, 4, 127.

Mochkovitch, R. 1980, private communication.

Pandharipande, V.R., and Smith, R.A. 1975a, Nucl. Phys., A237, 507.

_____ 1975b, Phys. Letters, 59B, 15.

Ramaty, R., Bonazzola, S., Cline, T.L., Kazanas, D., and Meszaros, P. 1980, Nature, 287, 122.

Rosen, L.C. 1969, Ap. Space Sci., 5, 150.

Ruderman, M. 1981, Prog. Part. Nucl. Phys., 6, 215.

Salpeter, E.E., and Van Horn, H.M. 1969, Ap.J., 155, 183.

Schrijver, J., Brinkman, A.C., Heise, J., den Broggende, A.J.F., Gronenschild, E.H.B.M., Mewe, R., Grindlay, J.E., and Parsignault, D.R. 1978, Astr. Ap., 69, L1.

Taam, R.E. 1980a, Ap.J., 241, 358.

_____ 1980b, preprint.

_____ 1980c, preprint.

Taam, R.E., and Picklum, R.E. 1978, Ap.J., 224, 210.

_____ 1979, Ap.J., 233, 327.

Van Horn, H.M., and Hansen, C.J. 1974, Ap.J., 191, 479.

Wallace, R.K., and Woosley, S.E. 1981, Ap.J. Suppl., 45, 389.

Weaver, T.A., Zimmerman, G.B., and Woosley, S.E. 1978, Ap.J., 225, 1021 (WZW).

Whyte, C.A., and Eggleton, P.P. 1980, M.N.R.A.S., 190, 801.

Woosley, S.E., Holmes, J.A., Fowler, W.A., and Zimmerman, B.A. 1978, Atomic Data and Nuclear Data Tables, 22, 371.

Woosley, S.E., and Taam, R.E. 1976, Nature, 263, 101.

Woosley, S.E., and Wallace, R.K. 1981, Ap. J., in press.

FIGURE CAPTIONS

FIG. 1. – Figure 1a shows the Temperature and density in the envelope of Model A when L has just reached 10^{38} erg s^{-1} ($t \sim 5$ μs). Here $R_p = 14.319$ km is the photospheric radius, and $M_* = 1.41\ M_\odot$ is the total mass of the star, so that $M_* - M(r)$ is the amount of mass exterior to radius r. Discontinuities are present at the composition boundaries between the hydrogen shell (right hand portion of the diagram), the helium shell, and the iron substrate. Figure 1b shows the composition of the envelope at the same time, with abundances given by mass fraction.

FIG. 2. – Thermodynamic structure and composition of the envelope in Model B when the luminosity just reaches 10^{38} erg s^{-1}. Here the photospheric radius R_p is 14.410 km, and the axes are as defined in Figure 1. The helium eventually burns completely to ^{56}Ni, which decays to ^{56}Fe.

FIG. 3. – Figure 3a shows the bolometric light curve for Model B. The precise photospheric evolution could not be obtained during the wind phase, so for this period the Eddington luminosity is indicated by the dashed line (essentially coincident with the data points). At three times during the wind phase, the course model was finely zoned, and the resulting luminosities are plotted as data points. The inset shows the initial luminosity rise in more detail, illustrating a rise time on the order of milliseconds. Figure 3b gives the effective temperature (T_{eff}; solid) and photospheric radius (R_p; dash dot) evolution for the event.

The luminosity of the finely zoned models remained constant at the Eddington value; however, the radius continued to increase, so only lower limits to the radius (and hence upper limits to T_{eff}) are shown as data points during the wind phase. Dashed lines during that time indicate the qualitative behavior of R_p and T_{eff}.

FIG. 4. - The substantially super Eddington luminosity at the base of the photosphere (r0 = 14.35 km) indicates the large amount of energy stored in the gravitational potential of the expanding photosphere during the wind phase of Model B.

FIG. 5. - As the outer envelope in Model B was more finely zoned, the apparent photospheric radius rapidly increased. Once this transient response to the abrupt rezoning had passed, the photosphere still continued to expand gradually with time. The points where the radius ceased its rapid increase were taken as the lower limits for R_p plotted in Figures 3 and 9 (i.e. the point at t = 192 ms in Figure 5 was used in Figure 3).

FIG. 6. - Some thermodynamic quantities in the envelope of a finely zoned calculation for Model B at t = 33.197 s. The sound speed is $c_s = \sqrt{\gamma P/\rho}$, where $\gamma = 4/3$, and the gas sonic speed is $c_{sg} = \sqrt{P_g/\rho}$. The photosphere is roughly at 45 km, with $T_{eff} \simeq 11.8 \times 10^6$ K, and a surface luminosity of 2.72×10^{38} erg s^{-1}.

FIG. 7. - Thermodynamic conditions and abundances in Model C just after the shock reached the surface. The axes are defined as in Figure 1, but with $R_p = 14.309$ km here. Temperatures as high as 6×10^9 K were reached at the base of the helium shell, and surface velocities

exceeding 10^{10} cm s^{-1} were produced. Again, all the helium eventually burned to ^{56}Ni, which later decayed to ^{56}Fe.

FIG. 8. - Radius and temperature at the boundary of several representative mass regions in the envelope during the rise in surface luminosity of Model C. The mass indicated is that mass external to the given zone boundary. The original radius of the cold neutron star was 14.3 km, so ~ 10^{24} g of material have been pushed above the original surface at this time.

FIG. 9. - Figure 9a shows the bolometric light curve for Model C. The Eddington luminosity is again indicated by a dashed line during the wind phase, and results of two finely zoned models are shown as data points. Figure 3b gives the effective temperature (T_{eff}; solid) and photospheric radius (R_p; dash-dot) evolution for the event. Dashed lines during the wind phase indicate the qualitative behavior of R_p and T_{eff}, and upper and lower limits obtained from the finely zoned models are shown as arrows. The γ ray spike produced as the shock wave broke through the surface is shown in the inset, and the luminosity at shock breakout follows the same evolution as the effective temperature, since the radius had not yet begun to increase.

FIG. 10 Neutrino luminosity evolution for Model C. Neutrino emission was the dominant cooling mechanism, with a total energy of 1.47×10^{43} erg emitted in neutrinos. Beyond about 6000 s, the curve is dashed, since the contribution from $^{56}Ni(e\ \nu)^{56}Fe$ (at a rather uncertain rate) is comparable to that from plasma processes.

FIG. 11. - Temperature, density, and envelope mass for stable hydrogen burning envelopes as a function of mass accretion rate $\dot{M}$ and metallicity. M_β is the amount of material burning by the β-limited CNO cycle, which is about 95% of the entire hydrogen envelope mass. Temperature and density curves for Z = 0.02, Z = 0.002, and Z = 0.0002 are indicated in Figure 11a by solid, dashed, and dash-dot lines respectively. Curves for Z = 9×10^{-4} and 4×10^{-5} are indicated in Figure 11b by solid and dashed lines respectively. All curves stop on the left of the diagrams where the CNO cycle ceases to be β-limited, so that a stable configuration may not exist. The conditions suggested in these diagrams should also not be used for $\dot{M} > \dot{M}_c$, which is the accretion rate where the hydrogen and helium burning shells overlap, and a hydrogen/helium runaway is likely to occur (Taam 1980c). $\dot{M}_c$ may be as high as 10^{-9} $M_\odot$/yr for Z = 0.02 or as low as 10^{-10} $M_\odot$/yr for Z = 4×10^{-4}. Data points show the stable hydrogen envelope parameters for the numerical models listed in Table 1.

FIG. 12. - Helium ignition curve, where the radiative diffusion cooling time (τ_R) equals the nuclear heating time ($\tau_{3\alpha}$), and a thermonuclear runaway is expected to occur. $M_* - M(r)$ is the mass contained in the helium shell whose density at the base is given by the left axis. The curve labeled b = 1.6 indicates where the theory used to calculate the electron screening factor for nuclear reactions breaks down. The line $\Gamma_{84} = 168$ indicates where the solid/liquid phase transition occurs for the $^8Be(\alpha,\gamma)^{12}C$ reaction, and a pycnonuclear theory would have to be used. The composition of the helium envelope was taken to be $X_\alpha = 1.0$.

Data points indicate conditions at the base of the helium shells given in Table 1 for the numerical models when the runaways initiated.

R. K. WALLACE: Group X-2, MS 220, Los Alamos National Laboratory, P.O. Box 1663, Los Alamos, NM 87545.

S. E. WOOSLEY: Lick Observatory, University of California, Santa Cruz, CA 95064.

T. A. WEAVER: Special Studies Group, L-372, Lawrence Livermore National Laboratory, Livermore, CA 94550.

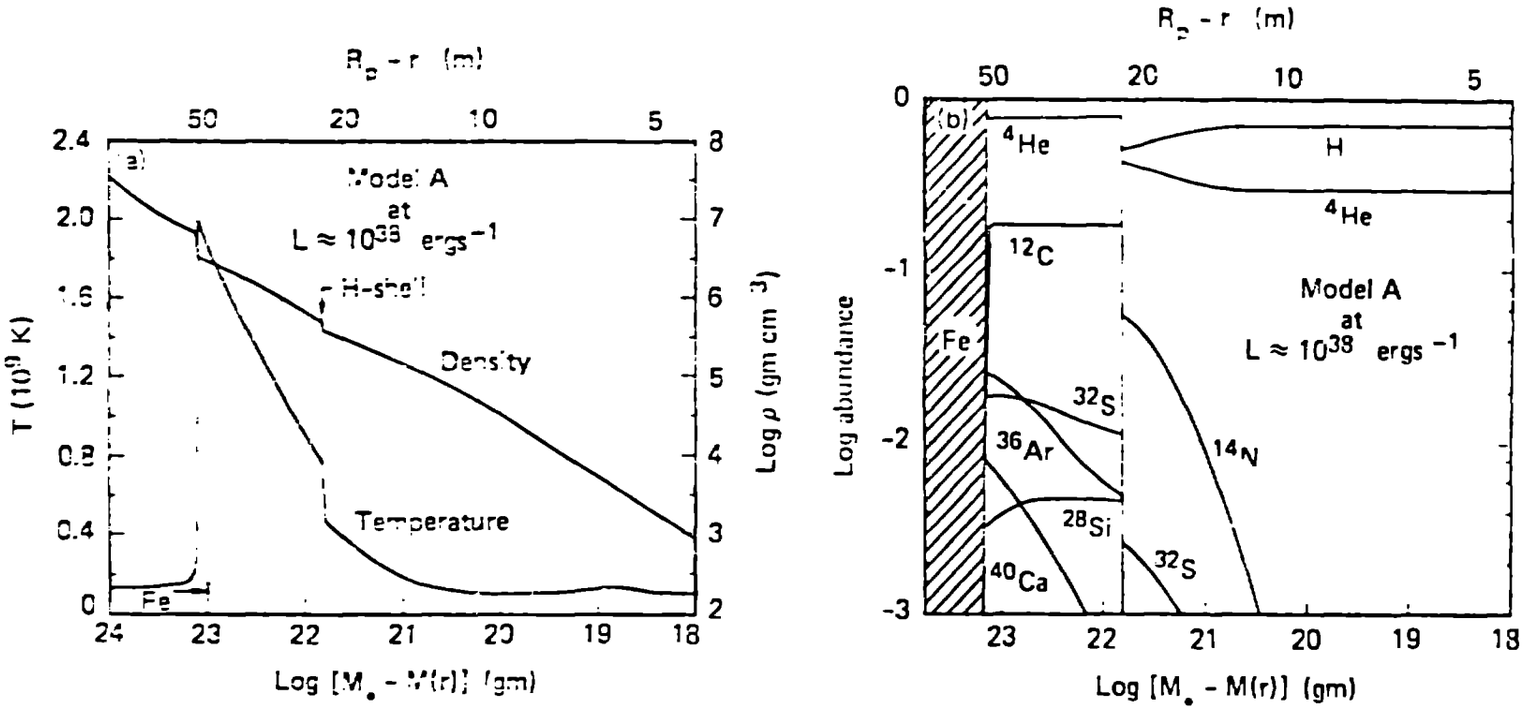
R_p - r (m)
50
20
10
5
(a)
Model A
at
L ≈ 10^38 ergs^-1
H-shell
Density
Temperature
Fe
T (10^9 K)
Log ρ (gm cm^-3)
Log [M_• - M(r)] (gm)
(b)
4He
H
4He
12C
Fe
32S
36Ar
14N
28Si
40Ca
32S
Log abundance

FIGURE 1

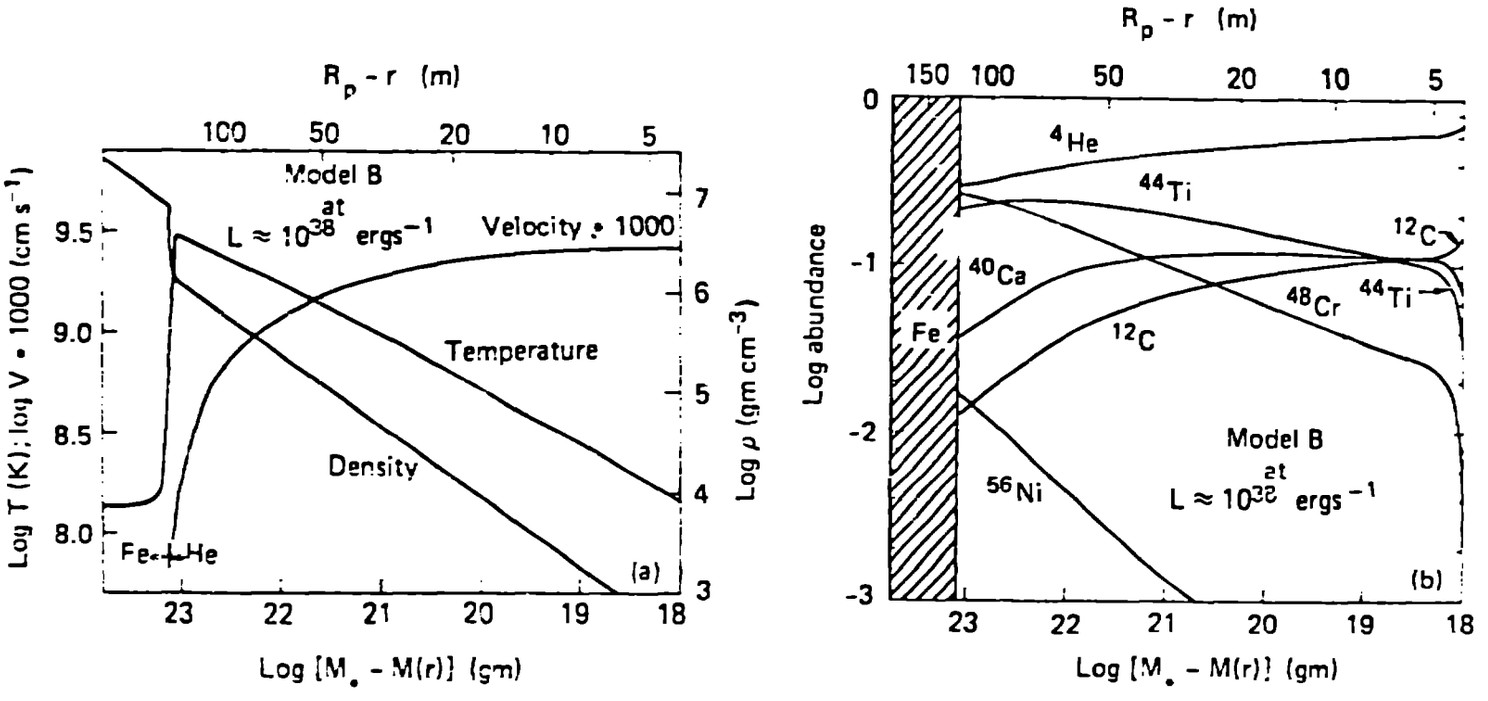
$R_p - r$ (m)
100 50 20 10 5
Model B
$L \approx 10^{38}$ ergs^{-1} at
Velocity • 1000
Temperature
Density
Fe + He
(a)
Log T (K); log V • 1000 (cm s^{-1})
Log ρ (gm cm^{-3})
Log [M_* - M(r)] (gm)
$R_p - r$ (m)
150 100 50 20 10 5
^{4}He
^{44}Ti
^{12}C
^{40}Ca
^{48}Cr
^{44}Ti
Fe
^{12}C
Model B
$L \approx 10^{38}$ ergs^{-1} at
^{56}Ni
(b)
Log abundance
Log [M_* - M(r)] (gm)

FIGURE 2

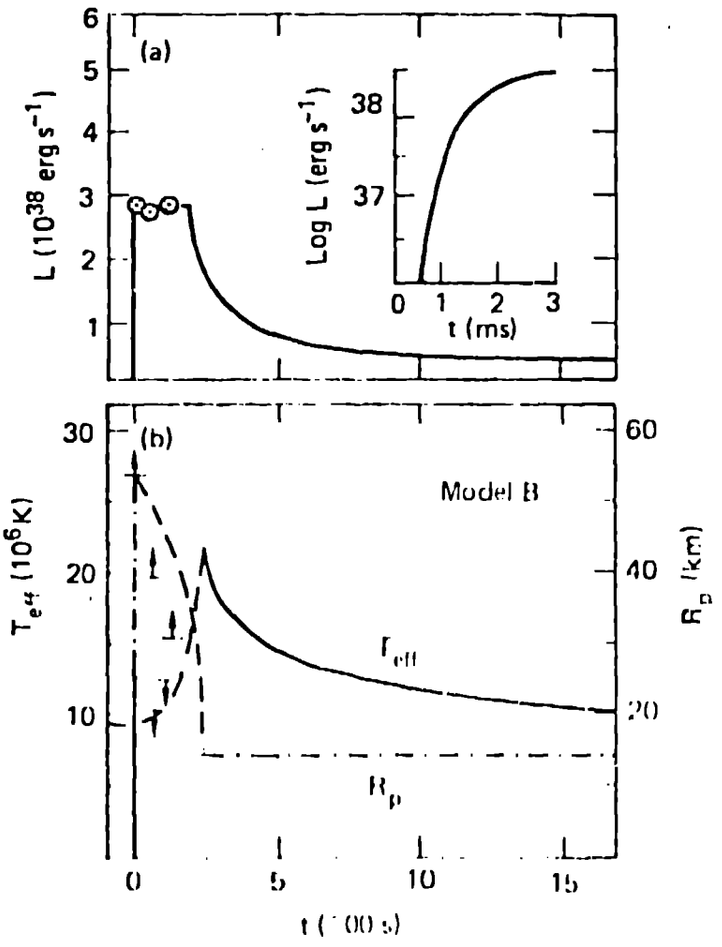
(a)
L (10^{38} erg s^{-1})
Log L (erg s^{-1})
38
37
0 1 2 3
t (ms)
(b)
Model B
T_{eff} (10^6 K)
R_p (km)
T_{eff}
R_p
0 5 10 15
t (100 s)

FIGURE 3

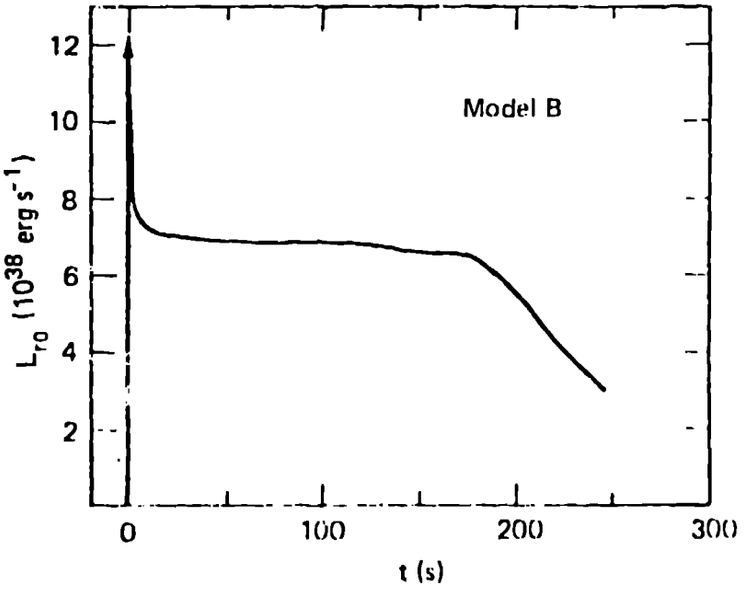

FIGURE 4

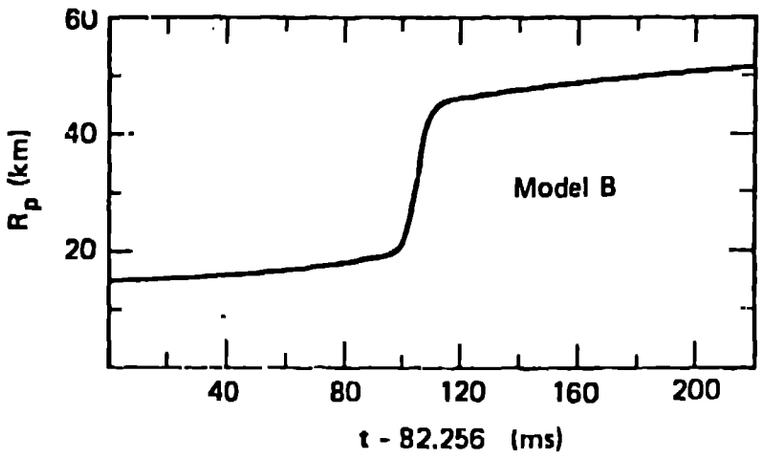

FIGURE 5

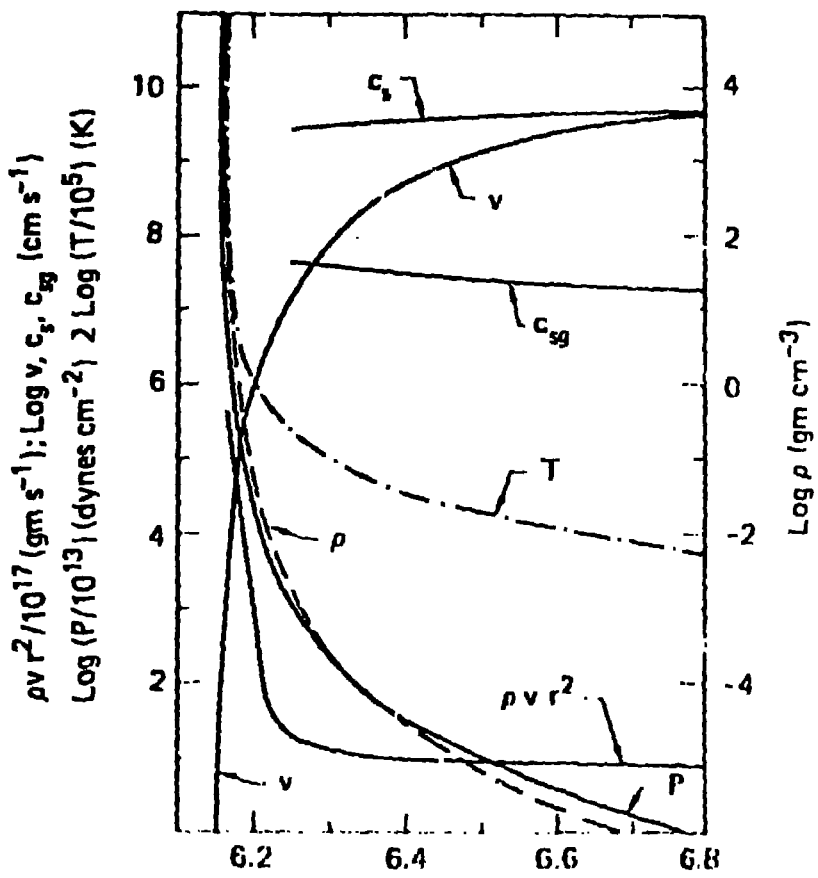
$\rho v r^2/10^{17}$ (gm s^{-1}); Log v, c_s, c_{sg} (cm s^{-1})
Log (P/10^{13}) (dynes cm^{-2}) 2 Log (T/10^5) (K)
Log ρ (gm cm^{-3})
c_s
v
c_{sg}
T
ρ
ρ v r^2
P
10
8
6
4
2
4
2
0
-2
-4
6.2
6.4
6.6
6.8
Log r (cm)

FIGURE 6

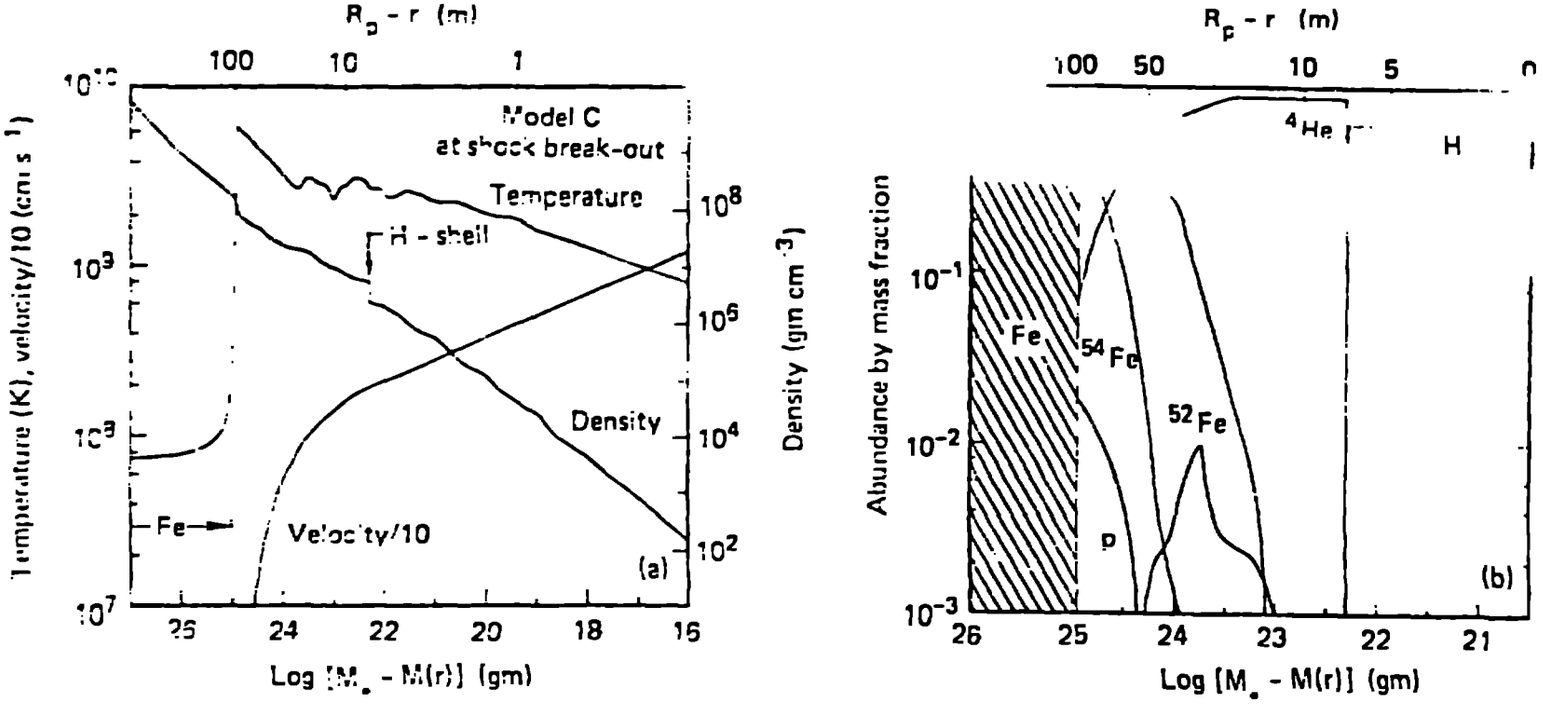
$R_p - r$ (m)
100
10
1
Model C
at shock break-out
Temperature
H - shell
Density
Fe
Velocity/10
(a)
Temperature (K), velocity/10 (cm s^{-1})
Density (gm cm^{-3})
10^{10}
10^9
10^8
10^7
10^6
10^4
10^2
25
24
22
20
18
16
Log [$M_\odot$ - M(r)] (gm)
$R_p - r$ (m)
100
50
10
5
0
^{4}He
H
Fe
^{54}Fe
^{52}Fe
p
(b)
Abundance by mass fraction
10^{-1}
10^{-2}
10^{-3}
26
25
24
23
22
21
Log [$M_\odot$ - M(r)] (gm)

FIGURE 7

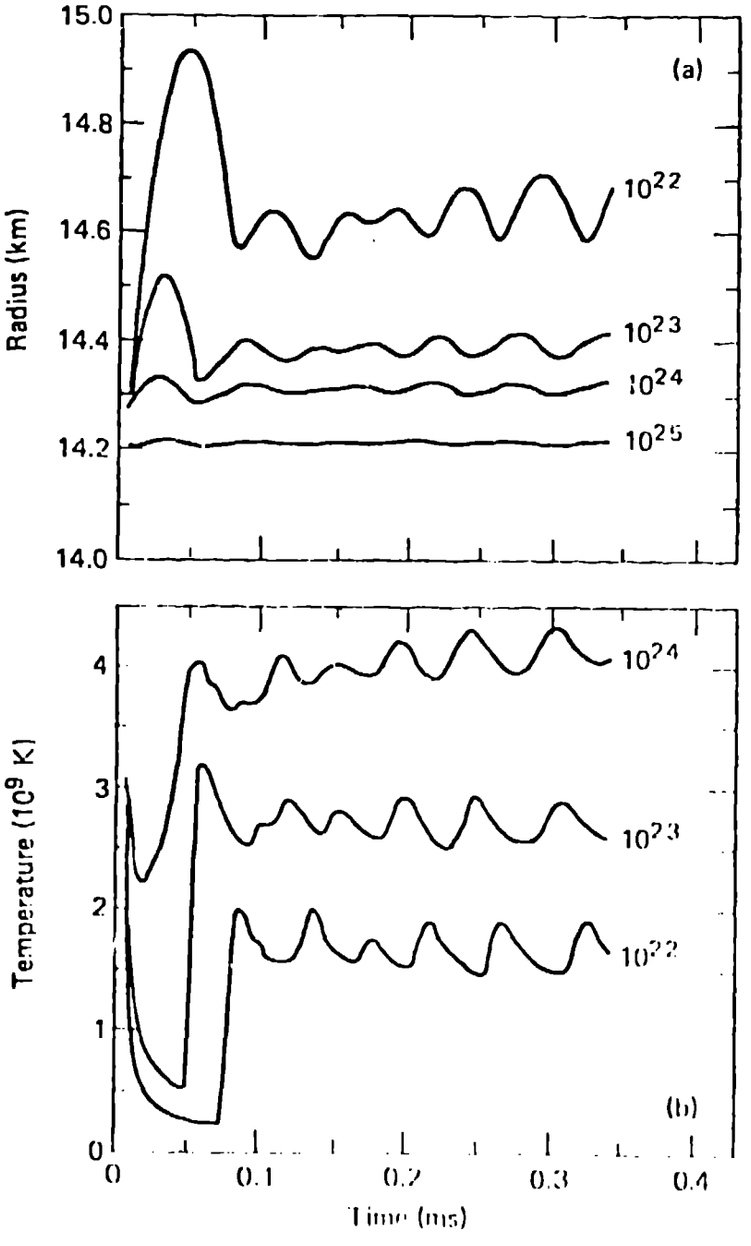
15.0
14.8
14.6
14.4
14.2
14.0
Radius (km)
(a)
10^{22}
10^{23}
10^{24}
10^{25}
4
3
2
1
0
Temperature (10^9 K)
10^{24}
10^{23}
10^{22}
(b)
0
0.1
0.2
0.3
0.4
Time (ms)

FIGURE 8

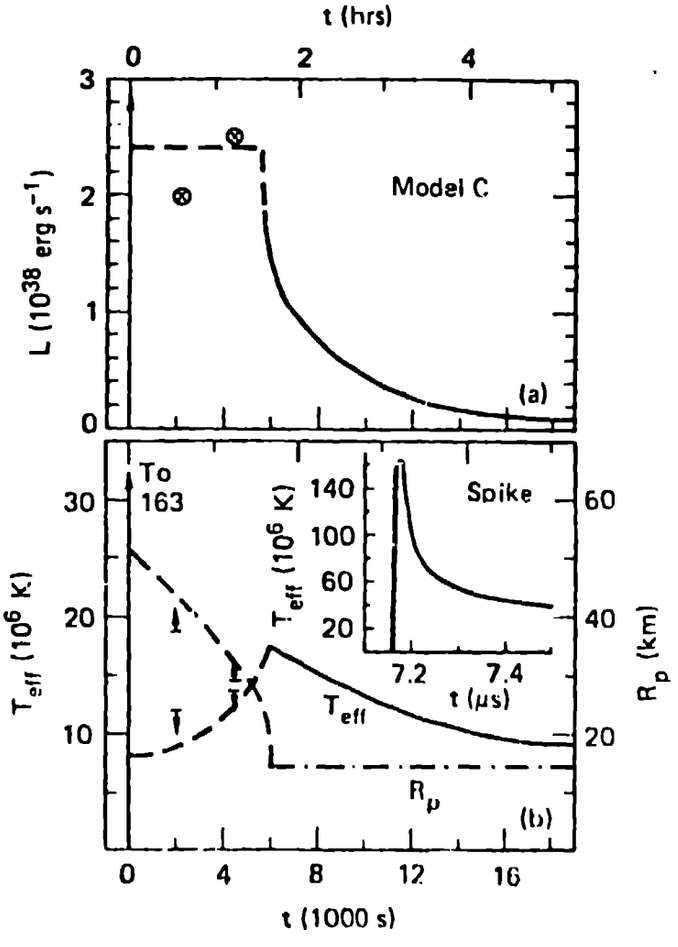
t (hrs)
0
2
4
3
2
1
0
L (10^{38} erg s^{-1})
Model C
(a)
To
163
30
20
10
T_{eff} (10^6 K)
140
100
60
20
T_{eff} (10^6 K)
Spike
7.2
7.4
t (μs)
T_{eff}
R_p
(b)
60
40
20
R_p (km)
0
4
8
12
16
t (1000 s)

FIGURE 9

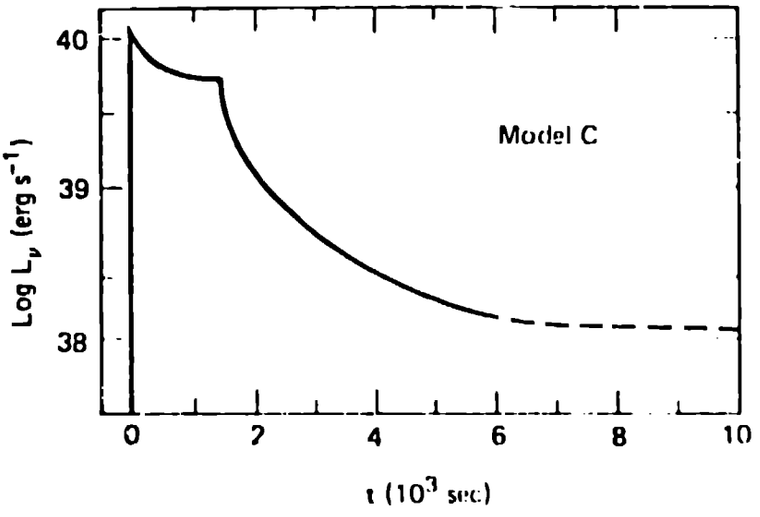

FIGURE 10

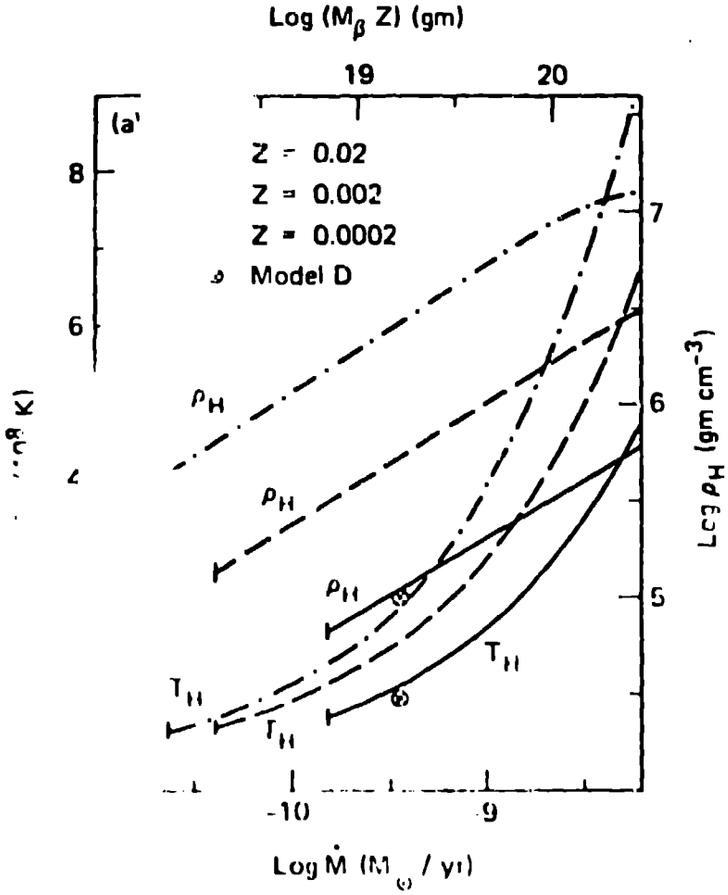
Log (M_β Z) (gm)
19
20
(a
Z = 0.02
Z = 0.002
Z = 0.0002
Model D
8
6
7
6
5
ρ_H
ρ_H
ρ_H
T_H
T_H
T_H
-10
-9
Log $\dot{M}$ ($M_\odot$ / yr)
Log ρ_H (gm cm^{-3})

FIGURE 11a

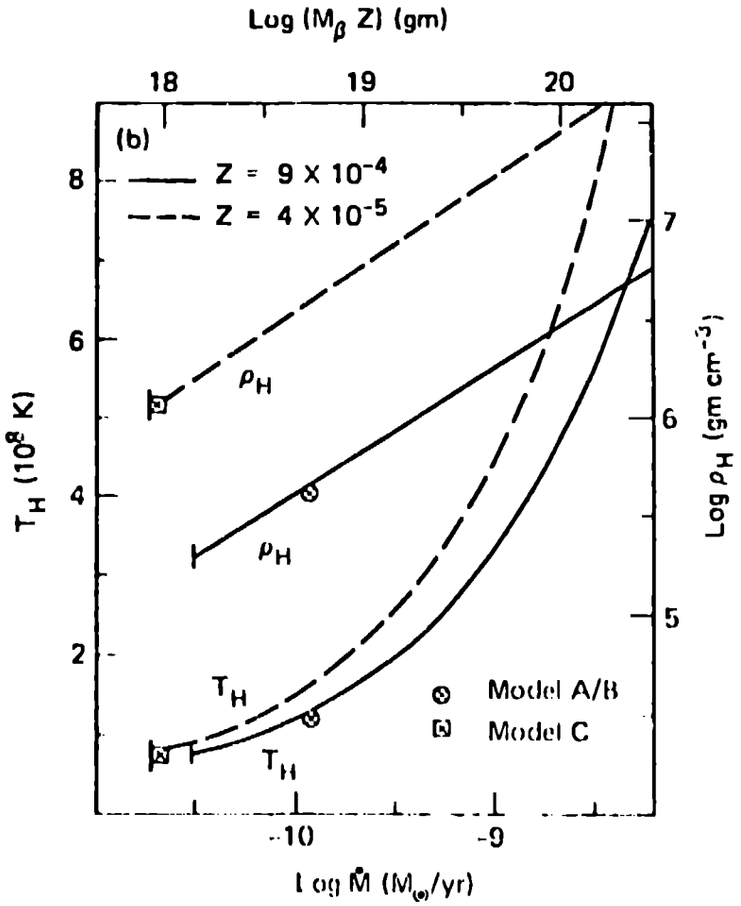
Log (M_β Z) (gm)
18
19
20
(b)
Z = 9 X 10^{-4}
Z = 4 X 10^{-5}
8
6
4
2
7
6
5
T_H (10^8 K)
Log ρ_H (gm cm^{-3})
ρ_H
ρ_H
T_H
T_H
Model A/B
Model C
-10
-9
Log $\dot{M}$ ($M_\odot$/yr)

FIGURE 11b

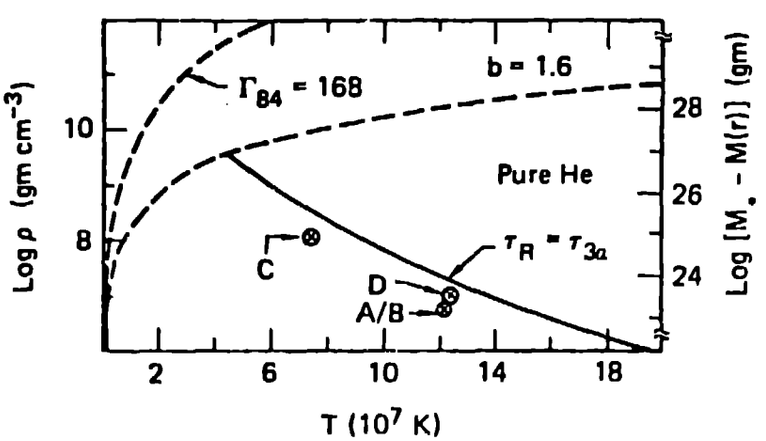
Log ρ (gm cm^{-3})
10
8
Γ_{84} = 168
b = 1.6
Pure He
$\tau_R = \tau_{3\alpha}$
C
D
A/B
2
6
10
14
18
T (10^7 K)
28
26
24
Log [M_* - M(r)] (gm)

FIGURE 12